LEGIBILITY NOTICE

A major purpose of the Technical Information Center is to provide the broadest dissemination possible of information contained in DOE's Research and Development Reports to business, industry, the academic community, and federal, state and local governments.

Although a small portion of this report is not reproducible, it is being made available to expedite the availability of information on the research discussed herein.

7/13/87 JS (2)

(5)

DE- 0289-5

I/31548

ORNL/TM-10374

ornl

OAK RIDGE
NATIONAL
LABORATORY

MARTIN MARIETTA

Studies of a Flexible Heliac Configuration

T. C. Hender
J. L. Cantrell
J. H. Harris
B. A. Carreras
V. E. Lynch
J. F. Lyon
J. A. Fabregas
J. Guasp
A. Lopez-Fraguas
A. P. Navarro

OPERATED BY
MARTIN MARIETTA ENERGY SYSTEMS, INC.
FOR THE UNITED STATES
DEPARTMENT OF ENERGY

Printed in the United States of America. Available from
National Technical Information Service
U.S. Department of Commerce
5285 Port Royal Road, Springfield, Virginia 22161
NTIS price codes—Printed Copy: A03; Microfiche A01

ORNL/TM--10374

DE87 013367

ORNL/TM-10374
Dist. Category UC-20

Fusion Energy Division

STUDIES OF A FLEXIBLE HELIAC CONFIGURATION

T. C. Hender*
J. L. Cantrell†
J. H. Harris
B. A. Carreras
V. E. Lynch†
J. F. Lyon

Fusion Energy Division, Oak Ridge National Laboratory

J. A. Fabregas
J. Guasp
A. Lopez-Fraguas
A. P. Navarro

Division de Fusion, Asociacion EURATOM/CIEMAT
Junta de Energia Nuclear
28040 Madrid, Spain

*Present address: Culham Laboratory, Abingdon, Oxfordshire, United Kingdom.
†Computing and Telecommunications Division, Martin Marietta Energy Systems, Inc.

Date Published - July 1987

Prepared by the
OAK RIDGE NATIONAL LABORATORY
Oak Ridge, Tennessee 37831
operated by
MARTIN MARIETTA ENERGY SYSTEMS, INC.
for the
U.S. DEPARTMENT OF ENERGY
under contract DE-AC05-84OR21400

CONTENTS

DISCLAIMER

ACKNOWLEDGMENTS

We are indebted to many of our colleagues at JEN and ORNL for numerous helpful discussions and suggestions. These studies have also benefited greatly from interactions with the stellarator group at IPP–Garching. This work was funded by the U.S.–Spain Committee for Scientific and Technological Cooperation. ORNL is operated by Martin Marietta Energy Systems, Inc., for the U.S. Department of Energy under contract DE-AC05-84OR21400.

ABSTRACT

This paper documents a detailed study of the Flexible Heliac configuration. The remarkable flexibility of this device — which allows variation of the rotational transform, shear, and magnetic well depth over a relatively wide range — is described. Engineering considerations of error fields, finite cross-section conductors, and plasma coil clearances are also discussed.

I. INTRODUCTION

The Flexible Heliac[1,2] (Fig. 1) consists of a toroidally directed central conductor, with a close-fitting $\ell = 1$ winding wrapped around it, and a set of toroidal field (TF) coils whose centers describe a helix that is concentric with the $\ell = 1$ winding; a set of outboard vertical field (VF) coils is also required for horizontal positioning. This coil set produces "bean-shaped" flux surfaces that follow the helical motion of the TF coils about the central conductors. A typical set of flux surfaces for the 4-field-period reference configuration described in this paper is shown in Fig. 2. It is the $\ell = 1$ winding that distinguishes the Flexible Heliac from the standard Heliac[3] and leads to the great flexibility in the device.

The Heliac has been found to have very favorable stability properties in the infinite-aspect-ratio, helically symmetric limit.[4] At finite aspect ratio, however, the high values of rotational transform per field period (ι/M) inherent to the Heliac can lead to equilibrium problems: the beating of the pressure-induced, toroidal Shafranov shift with the helical harmonics may produce resonant or nearly resonant harmonics that can distort or destroy the flux surfaces.[5] Such resonant effects

ORNL-DWG 85-2996 FED

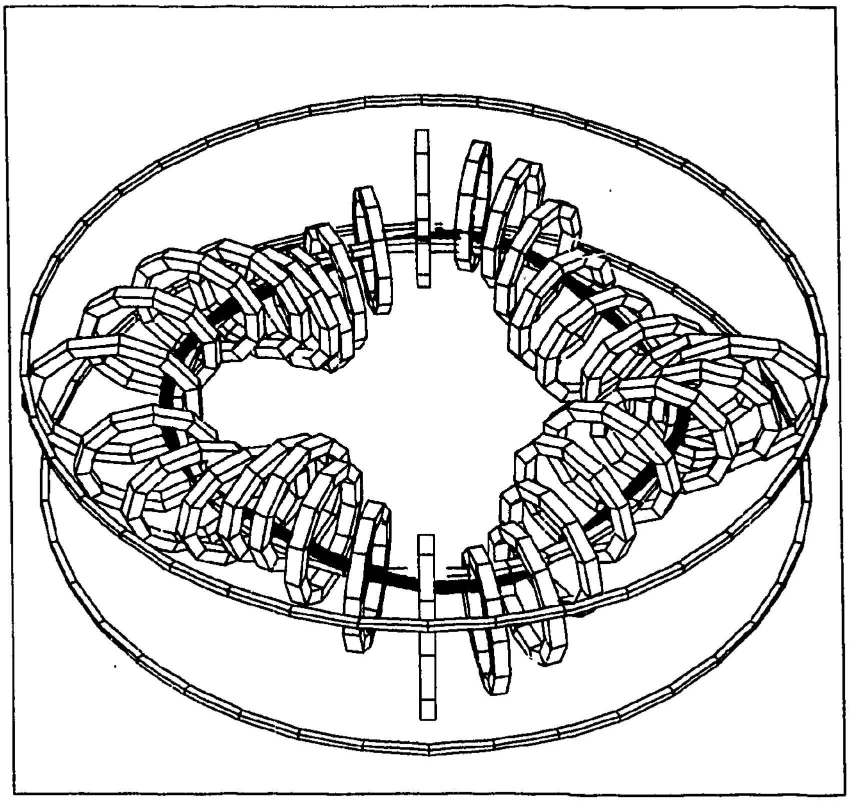

Fig. 1. Coil set for 4-field-period Flexible Heliac.

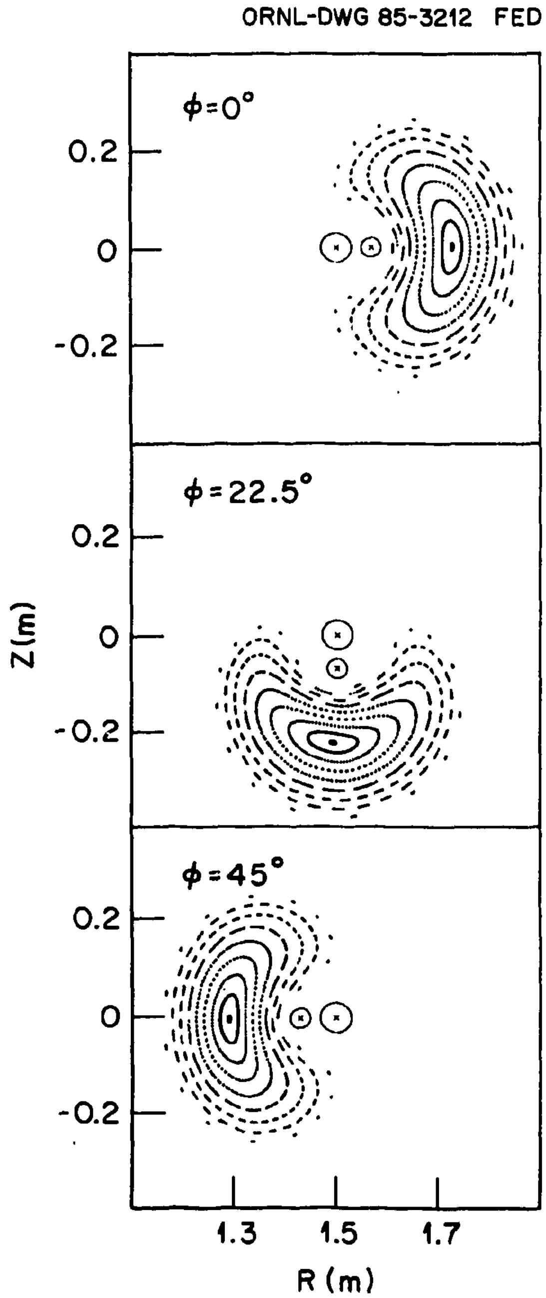

Fig. 2. Typical flux surfaces at four toroidal angles for the reference configuration.

are particularly pronounced when the plasma contains, or has nearby, low-order resonant surfaces.[6] It is thus very important for a Heliac experiment to have sufficient control over the rotational transform and shear to avoid the low-order resonances. Conversely, it will also be interesting to examine plasma properties in the vicinity of low-order resonances in the hope of improving theoretical understanding.

There are some theoretical indications that the magnetic well depth may play an important role in determining the growth and magnitude of the equilibrium-induced resonant harmonics.[7] It is thus also desirable to be able to vary the magnetic well depth.

The Flexible Heliac satisfies these requirements for independent variation of the rotational transform, shear, and magnetic well depth. The concept has already undergone a basic test in low-temperature plasma experiments on the prototype SHEILA device,[8] which showed that the $\ell = 1$ winding can be effectively used to control the rotational transform so as to avoid the most dangerous low-order resonances. The reference configuration described here was chosen for study because it permits variation of the rotational transform over a wide range ($0.15 \lesssim \iota/M \lesssim 0.8$); at fixed values of ι, the shear and magnetic well depth may also be varied to a more limited extent. This particular configuration has been used as a basis for the design of the TJ-II Flexible Heliac,[9] which is proposed to be constructed in Madrid (Spain). Similar features are being incorporated in the H-1 device under construction in Canberra (Australia).[8]

The parameter scans and external constraints that led to the choice of the reference configuration are briefly described in Sec. II. The physics properties of the reference case are explored in detail in Sec. III. Practical studies of error fields, the effects of finite cross-section conductors, and plasma coil clearances are described in Sec. IV. A summary is given in Sec. V.

II. CONFIGURATION SCANS

As discussed in Sec. I, one of the chief theoretical concerns in the Heliac relates to the possibility that equilibrium flux surfaces may be destroyed at finite beta.[5] This flux surface destruction arises from resonant or nearly resonant magnetic perturbations, which are generated by the nonlinear beatings of the toroidal and helical shifts (and by subsequent higher order beatings).

Since the helical curvature is intrinsic to the Heliac, the only way to reduce the magnitude of nonlinearly driven resonant fields (and thus the improve the equilibrium beta limit) is to reduce the toroidal shift. At relatively tight aspect ratios ($\lesssim 10$), this can be done by increasing the number of field periods and/or the aspect ratio.[10] Thus, from an equilibrium viewpoint it is clear that a large aspect ratio and a large number of field periods are desirable. However, cost constraints (which must be kept in mind for a practical design) act in the opposite direction and favor a small aspect ratio and number of field periods; a compromise is thus necessary. The chosen reference configuration has four field periods and a major radius of 1.5 m, which permits plasmas with an average radius of up to 25 cm and betas of at least 8%. Increasing the number of field periods and the coil aspect ratio proportionally improves the equilibrium properties linearly, but of course this leads to a reduction in the plasma minor radius (for fixed R). Similarly, increasing only the number of field periods improves the equilibrium properties but reduces the minor radius. Another problem with increasing the number of field periods beyond four is that access for heating and diagnostics is seriously reduced.

The swing radius of the TF coils sets the optimum ι range for the Heliac. Holding all other parameters fixed while increasing the TF coil swing radius decreases ι/M, and, conversely, reducing the swing radius raises ι/M. The chosen swing radius, $r_S = 28$ cm, leads to optimum plasma volumes near $\iota/M \sim 0.4$, although varying the relative currents in the circular and helical hardcore windings allows wide variations of ι/M about this "optimum" value. A lower bound on the swing radius of the helical hardcore (r_{hc}) is imposed by the cross-sectional areas of the two central conductors, which are necessary to carry the required currents. For the reference value of $r_{hc} = 7$ cm, each conductor can carry up to 300 kA. This assumes that the helical conductor is tightly wrapped on the central conductor and that each has a 3.5-cm radius. Increasing the swing radius of the helical conductor improves the efficiency with which the required helical fields are generated. However, there is at best limited clearance between the $\ell = 1$ (helical hardcore) winding and the plasma, and some form of limiter may be necessary to protect the winding for some of the variations that can be achieved with the reference configuration. Increasing the $\ell = 1$ winding swing radius further would reduce the plasma-coil clearance and limit the plasma minor radius even more.

The effects of varying the radii of the TF coils while holding all other parameters fixed are shown in Fig. 3. For coil radii less than 40 cm, the plasma-coil clearances at the tips of the plasma "bean" are insufficient, while for radii much greater than 40 cm there is a slow decrease in plasma radius.

The configuration properties are weakly dependent on the number of TF coils per field period. Increasing the number of TF coils yields a slow improvement in flux surface quality and plasma minor radius (Fig. 4) and also leads to deeper magnetic wells (Fig. 5). Eight coils per field period were chosen as a compromise between physics properties, plasma access, and engineering feasibility.

To summarize, the parameters for the reference configuration were selected on the basis of systematic single-parameter scans about an $R = 1.5$ m, 4-field-period case. The chosen configuration consists of 32 TF coils that are helically displaced by 28 cm from the hardcore winding, with the winding law $\theta = 4\phi$. The hardcore itself is composed of a circular coil of 1.5 m radius and a helical $\ell = 1$ winding that follows the same winding law as the TF coils, but with a smaller, 7-cm swing radius. The nominal toroidal field is taken to be 1 T, which is consistent with requirements for electron cyclotron resonance heating (ECRH) at 28 GHz (fundamental) and 56 GHz (second harmonic). The two outboard VF coils located at $R = 2.25$ m and

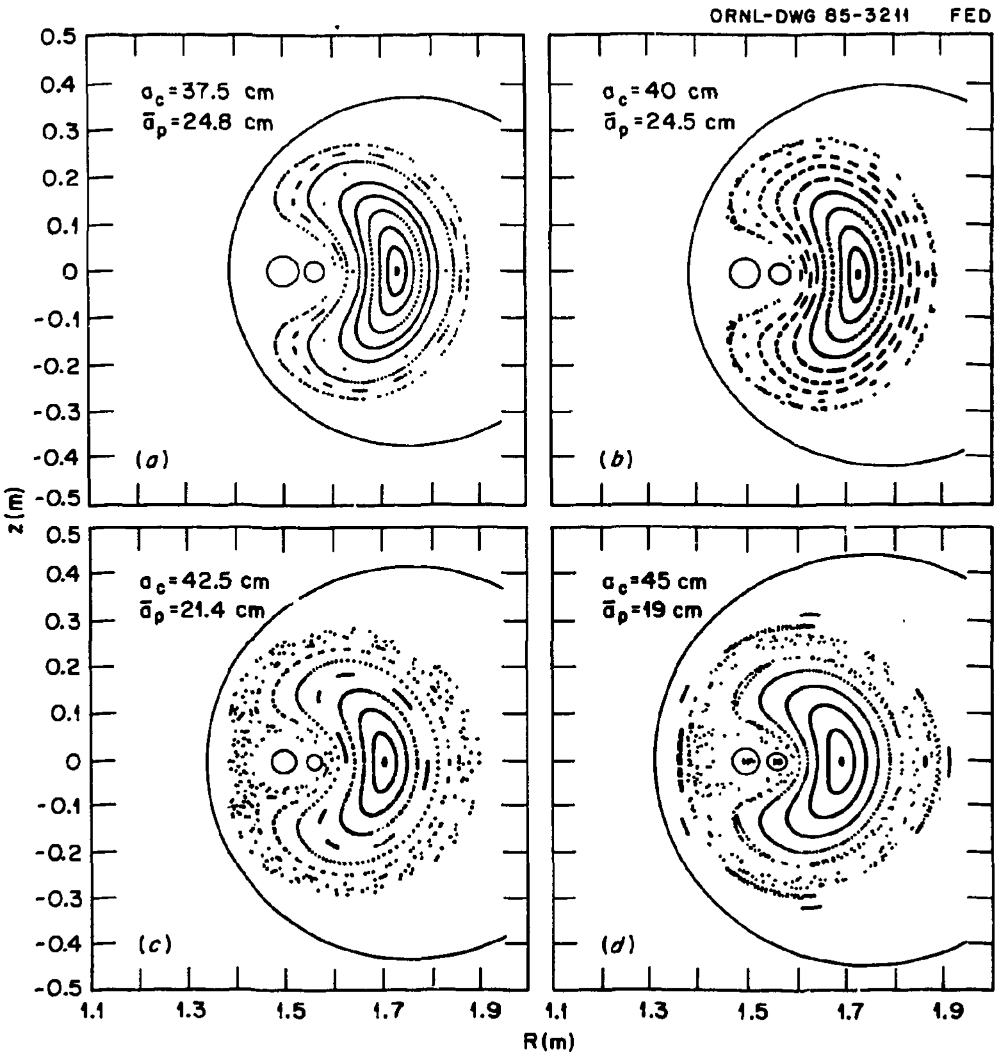

Fig. 3. Effect of varying the TF coil radius (a_c) on the average plasma radius ($\bar{r}$).

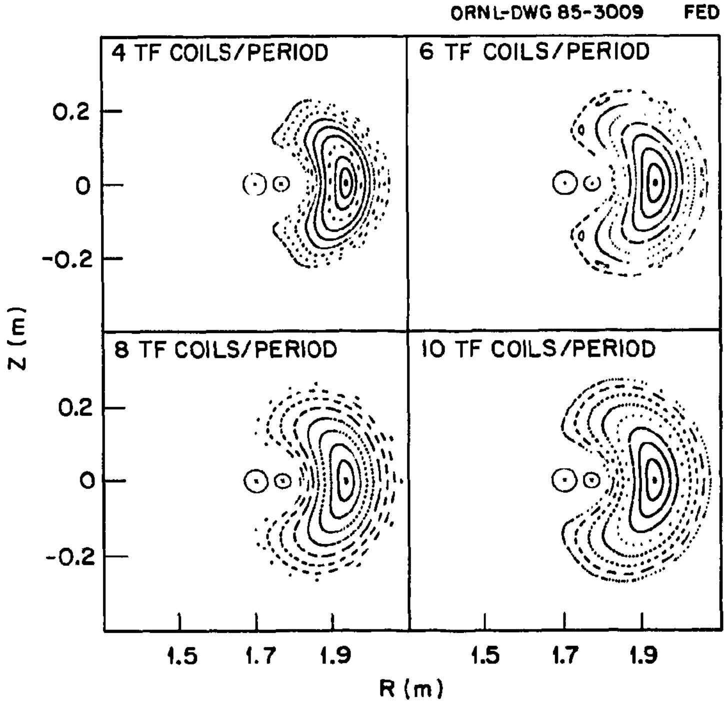

Fig. 4. Effect of increasing the number of TF coils per field period on flux surface quality.

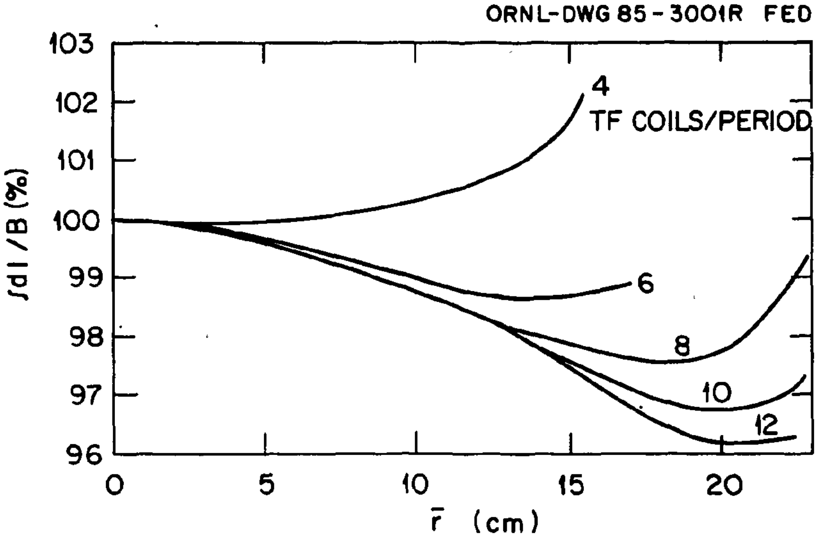

Fig. 5. Effect of increasing the number of TF coils per field period on the magnetic well depth.

$z = \pm 0.4$ m are required to position the plasma and contribute vertical fields of ~5% of the toroidal field strength. The parameters for the reference configuration are summarized in Table I.

TABLE I
Reference Configuration Parameters

Winding law	$\theta = 4\phi$
Major radius	1.5 m
TF coil radius	0.4 m
TF coil swing radius	0.28 m
$\ell = 1$ winding swing radius	0.07 m
VF coil location	$R = 2.25$ m, $Z = \pm 0.4$ m
Maximum central coil current	300 kA
Nominal TF coil current	234 kA
VF coil current range	60–100 kA

III. PHYSICS PROPERTIES

The physics properties of the configuration detailed in Sec. II (and Table I) are described.

Figure 6 illustrates the remarkable flexibility that is achievable in the reference configuration. It shows contours of constant central rotational transform per field period (ι_0/M) as a function of the central conductor current (I_{cc}) and helical conductor current (I_{hc}). The value of ι_0 can be varied by a factor of ~5 between a lower limit of ~0.15 and an upper limit of ~0.8. The central conductor currents shown in Fig. 6 (<300 kA) are practical with current densities of 10 kA/cm^2.

Figure 7 shows a variety of flux surface plots for various ι/M, and Fig. 8 shows a selection of ι profiles. All of the reference configuration ι profiles have the low shear characteristic of helical-axis devices. The increasing bean shaping that occurs at higher ι_0/M (Fig. 7) leads to deeper magnetic wells. This is illustrated for three ι_0/M values in Fig. 9. It is also possible to vary the magnetic well depth at fixed ι_0/M by altering the mix of helical and central conductor currents. Figure 10 shows flux surfaces for $\iota_0/M = 0.36$ and 0.62. As the total central conductor current is increased with ι/M held fixed, the helical swing radius of the magnetic axis

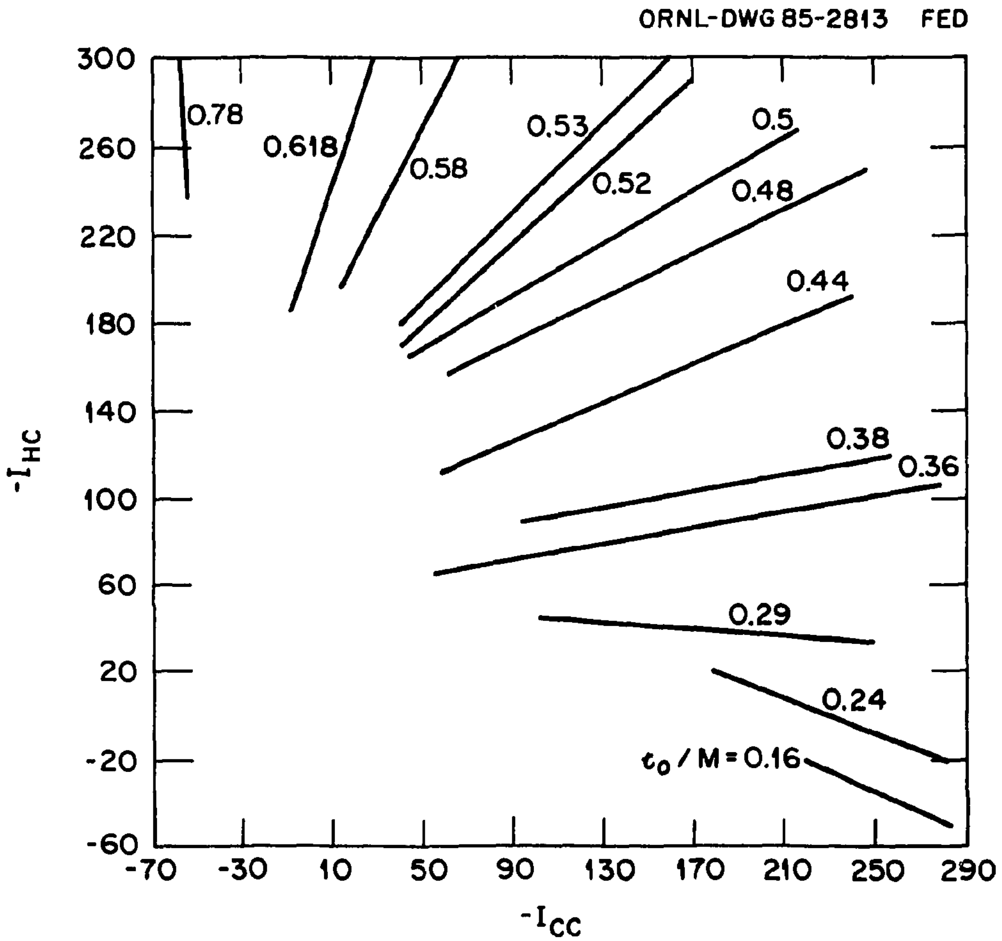

Fig. 6. Contours of constant ι_0/M as a function of central conductor (I_{cc}) and helical conductor (I_{hc}) currents.

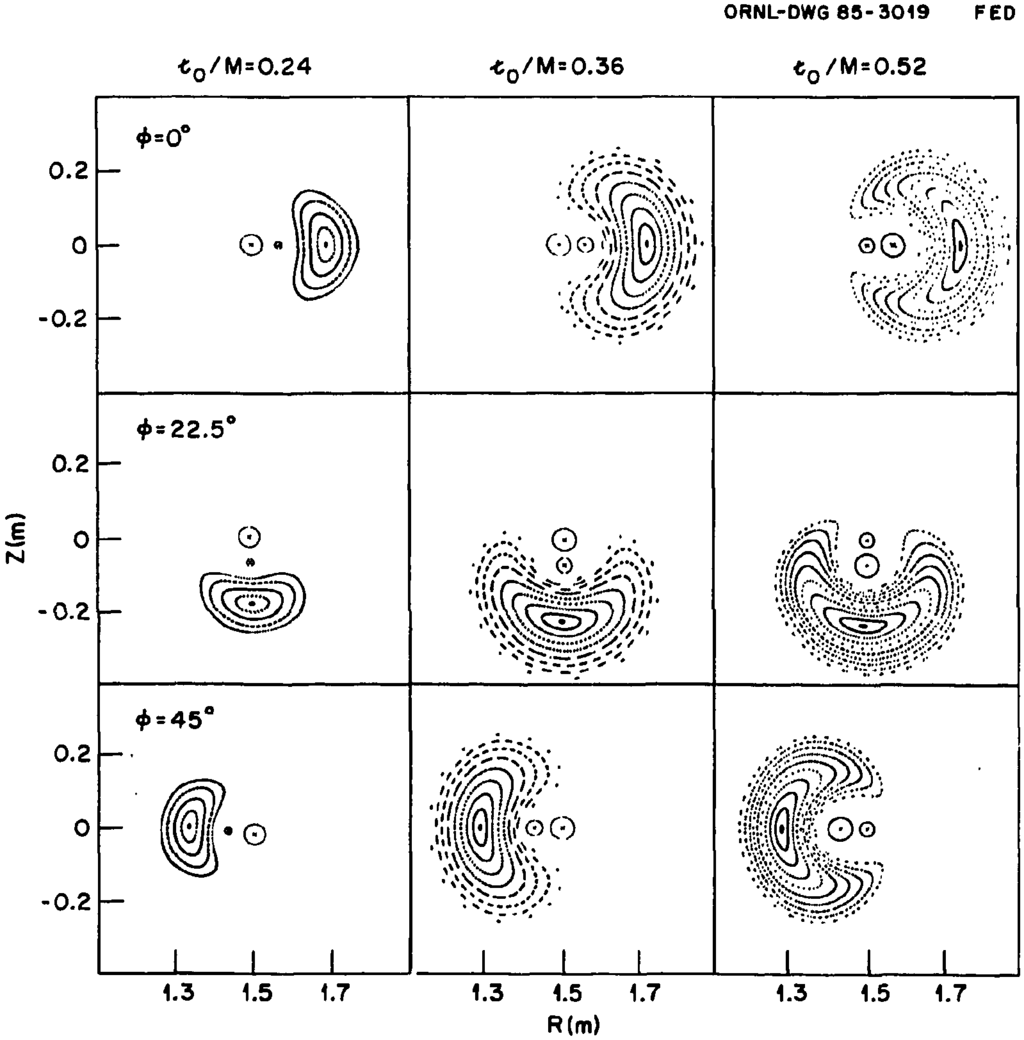

Fig. 7. Flux surfaces for several ι_0/M.

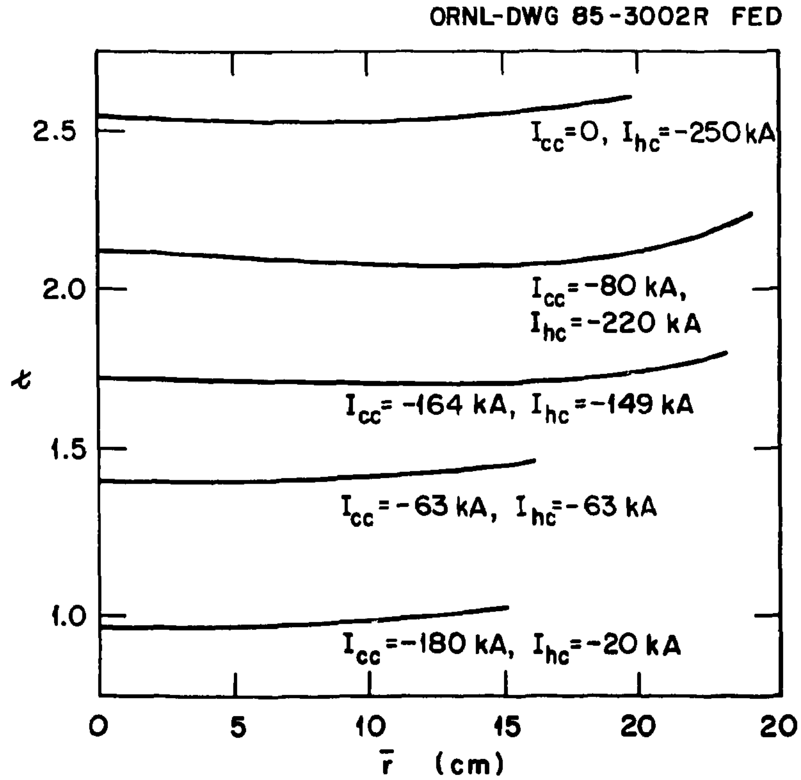

Fig. 8. Typical ι profiles for various central conductor currents.

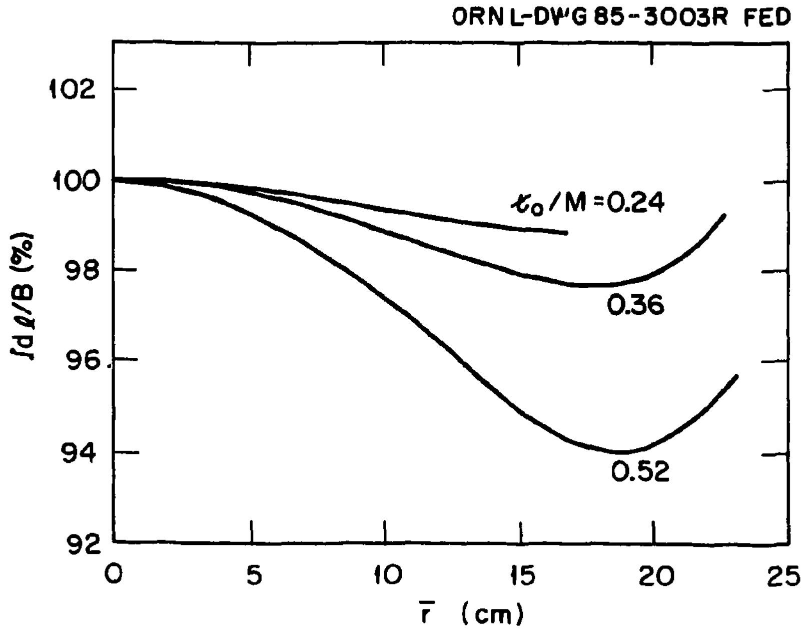

Fig. 9. Increase in magnetic well depth as ι_0/M increases.

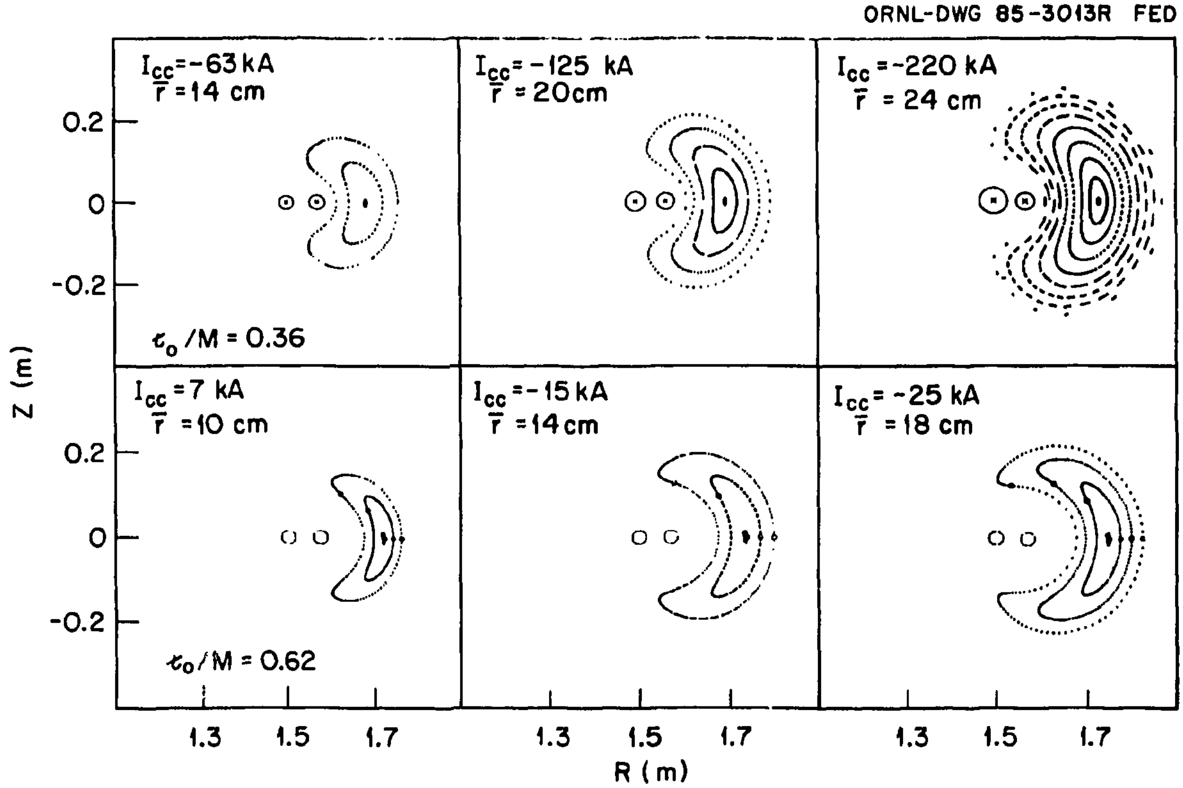

Fig. 10. Flux surfaces at $\iota_0/\mathrm{M} = 0.36$ (upper row) and 0.62 (lower row), showing increase in plasma volume at fixed ι_0/M as the central conductor current is increased.

increases, and there is a corresponding increase in average plasma minor radius. As the magnetic axis moves away from the hardcore, the surface indentation (and thus the magnetic well depth) at a given average radius also decreases. This is shown for the $\iota_0/M = 0.36$ case in Fig. 11, where well depths for a range of hardcore currents are plotted. The higher current cases have shallower wells at a given average radius and at the highest currents actually have destabilizing curvature ($V'' > 0$) near the plasma edge.

Figure 12 shows how the average radius of the last closed flux surface varies in the I_{hc}–I_{cc} plane of Fig. 6. A comparison of Figs. 6 and 12 shows that for a given ι_0/M, the average plasma radius increases as the total central conductor current is increased. The major resonances ($\iota_0/M = 1/3, 1/2, \ldots$) also play a role in determining the average radius. As the transform is raised toward the resonance, the outer surfaces begin to break up, and the average plasma radius is reduced. However, the resonances can be approached very closely from above without affecting the average radius, since the shear is positive for most of the accessible configurations.

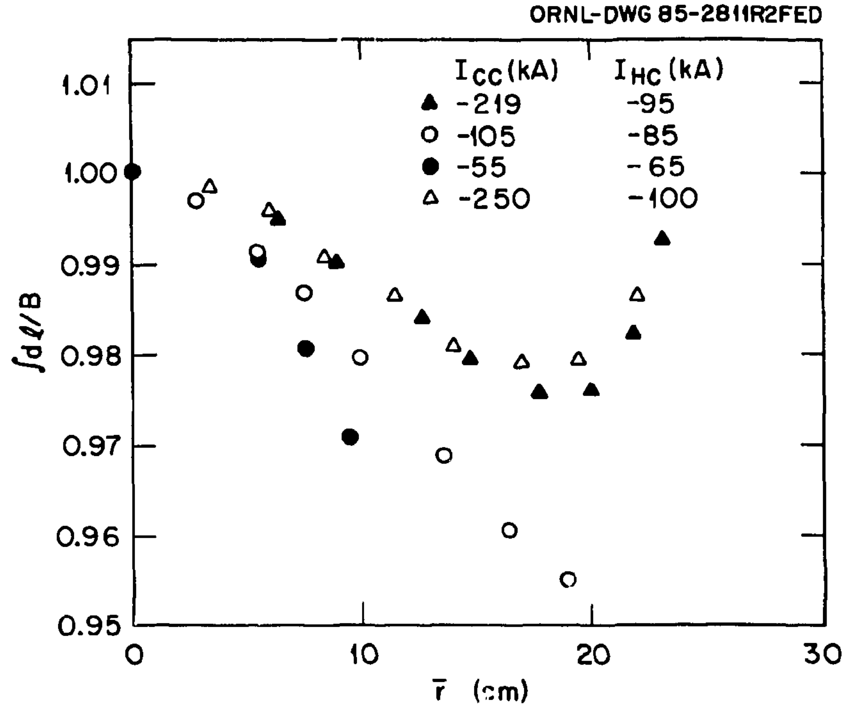

Fig. 11. Decrease in magnetic well depth as $(I_{cc} + I_{hc})$ is raised for the $\iota_0/M = 0.36$ case of Fig. 10.

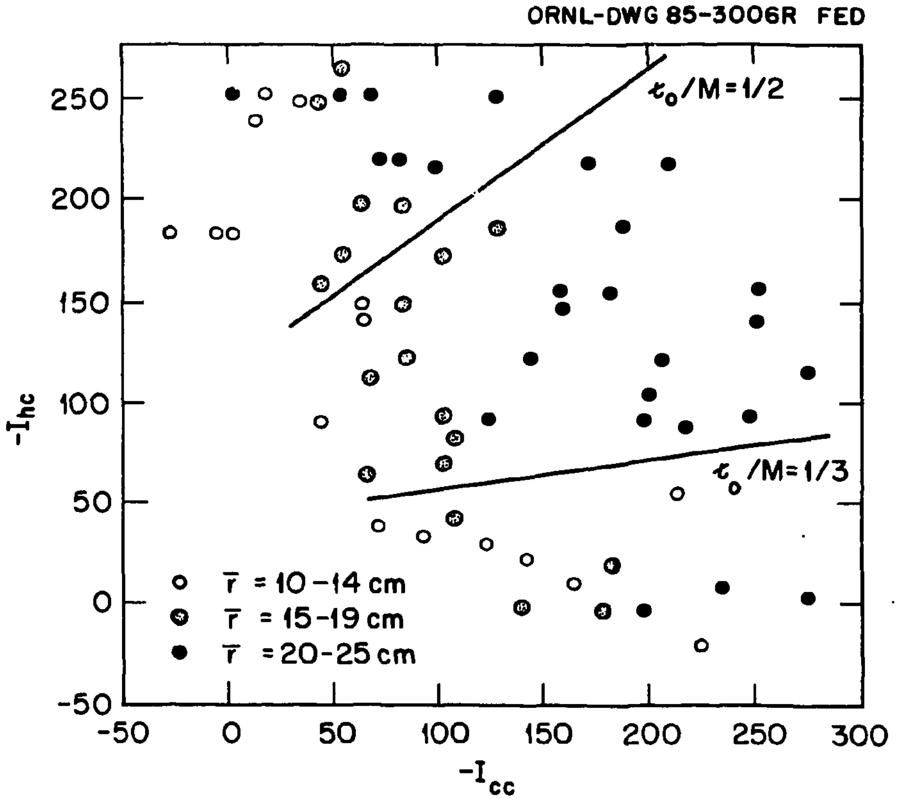

Fig. 12. Average plasma radii in the I_{cc}–I_{hc} plane.

At fixed ι_0/M, it is possible to control the shear to some degree by changing the hardcore currents. At high ι_0/M ($\geq$0.5) the shear tends to be lower and even slightly negative in some cases. Neither of these effects on the shear is particularly large; more importantly, they are not independent of the transform and well. A far greater degree of variation in the shear can be achieved by independently powering the inner and outer turns of the $\ell = 1$ winding. This allows the effective swing radius of the $\ell = 1$ winding to be varied between 5.25 cm and 8.75 cm for currents $I_{hc} < 150$ kA. Figure 13 shows the effect of shifting the centroid of the current over this range; significant (by Heliac standards) positive and negative shear can be achieved.

Another degree of freedom in the configuration can be achieved by modulating the currents in the TF coils according to their toroidal location:

$$I_{TF} = I_0(1 + C_F \cos 4\phi) \ . \tag{1}$$

This modulation directly affects the $m = 0$, $n = 4$ harmonic of the magnetic field and, by beating with the helical $m = 1$, $n = 4$ harmonic, can also affect the $m = 1$, $n = 0$ harmonic. Thus, in second order, the toroidal shift, which is proportional to the magnitude of $B_{1,0}^2$, can be reduced (or increased by this current

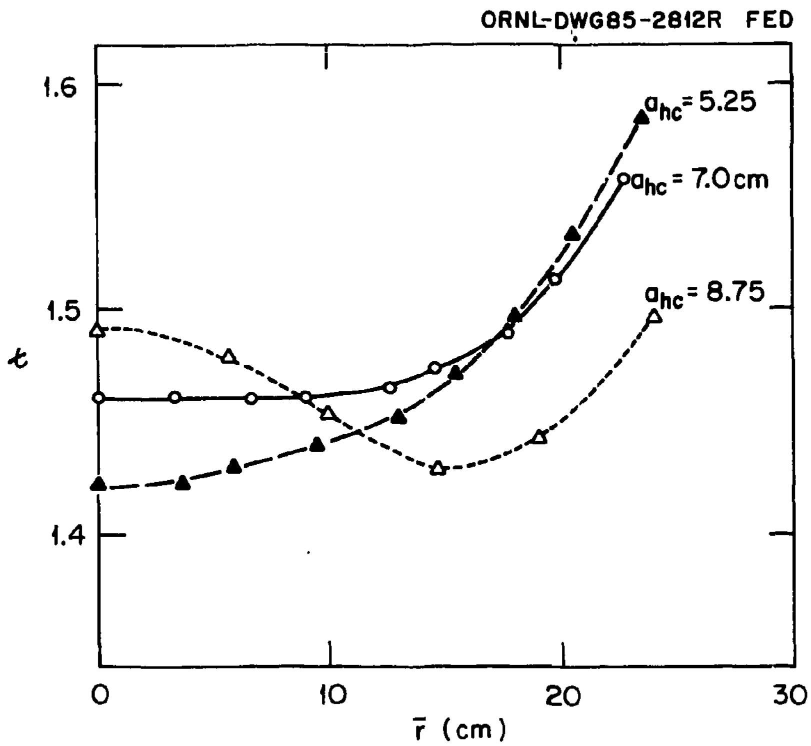

Fig. 13. Effect of shifting the centroid of the $\ell = 1$ winding current (a_{hc}) on the shear.

modulation. At the reference aspect ratio, however, the toroidicity is dominated by the $1/R$ dependence, and the effects of current toroidicity modulation alter $B_{1,0}^2$ by only ~10%.[8] A more important consequence of modulating the TF coil currents is the effect on the field ripple and thus the orbit losses. Figure 14 shows how the field ripple is altered by modulating the TF coil current between the limits +17% and −20%. It can be seen that the C_F = 17% modulation substantially reduces the field ripple near the magnetic axis. The flux surfaces corresponding to the range of current modulations of Fig. 14 are shown in Fig. 15. The requirement for conservation of the toroidal flux within a given surface causes the flux surface areas to be larger at $\phi = 0°$ than at $\phi = 45°$ when $C_F = 0$. This results from the underlying $1/R$ dependence of the toroidal field; applying a modulation C_F = 15% approximately compensates for the $1/R$ dependence, and the flux surface areas at these two cross sections are then nearly equal.

Many of the properties of the Flexible Heliac can be understood by studying a simple analytical model.[1] In the helically symmetric limit, the helical flux function[11–13] is

$$\psi = \frac{B_0}{R_0}\frac{r^2}{2} - \frac{\mu_0 I}{2\pi}\ln r - r\left[a_1 I_1'\left(\frac{r}{R_0}\right) + b_1 K_1'\left(\frac{r}{R_0}\right)\right]\cos\left(\theta - \frac{z}{R_0}\right) , \qquad (2)$$

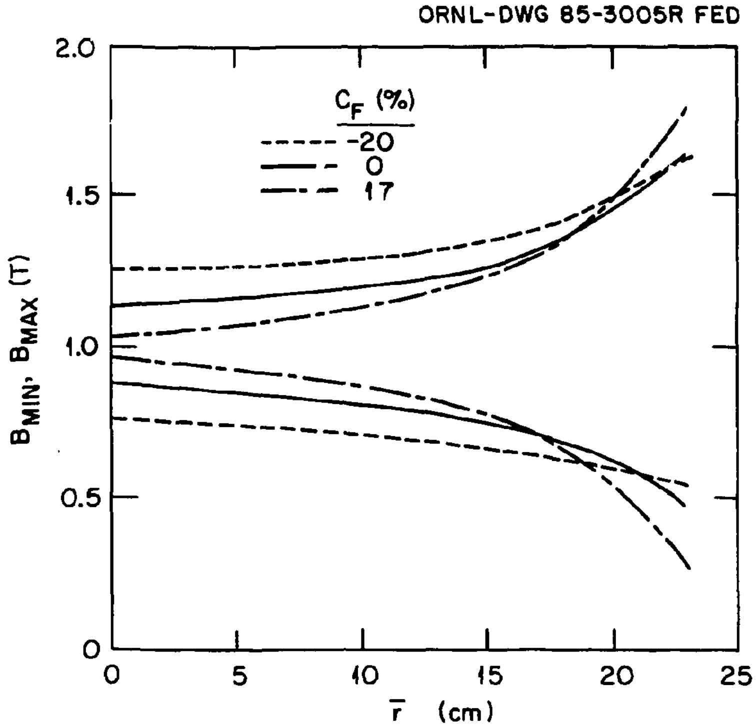

Fig. 14. Effect of changing the modulation (C_F) of the TF coil currents on the variation of $|\vec{B}|$ on a flux surface (labeled by average radius, $\bar{r}$).

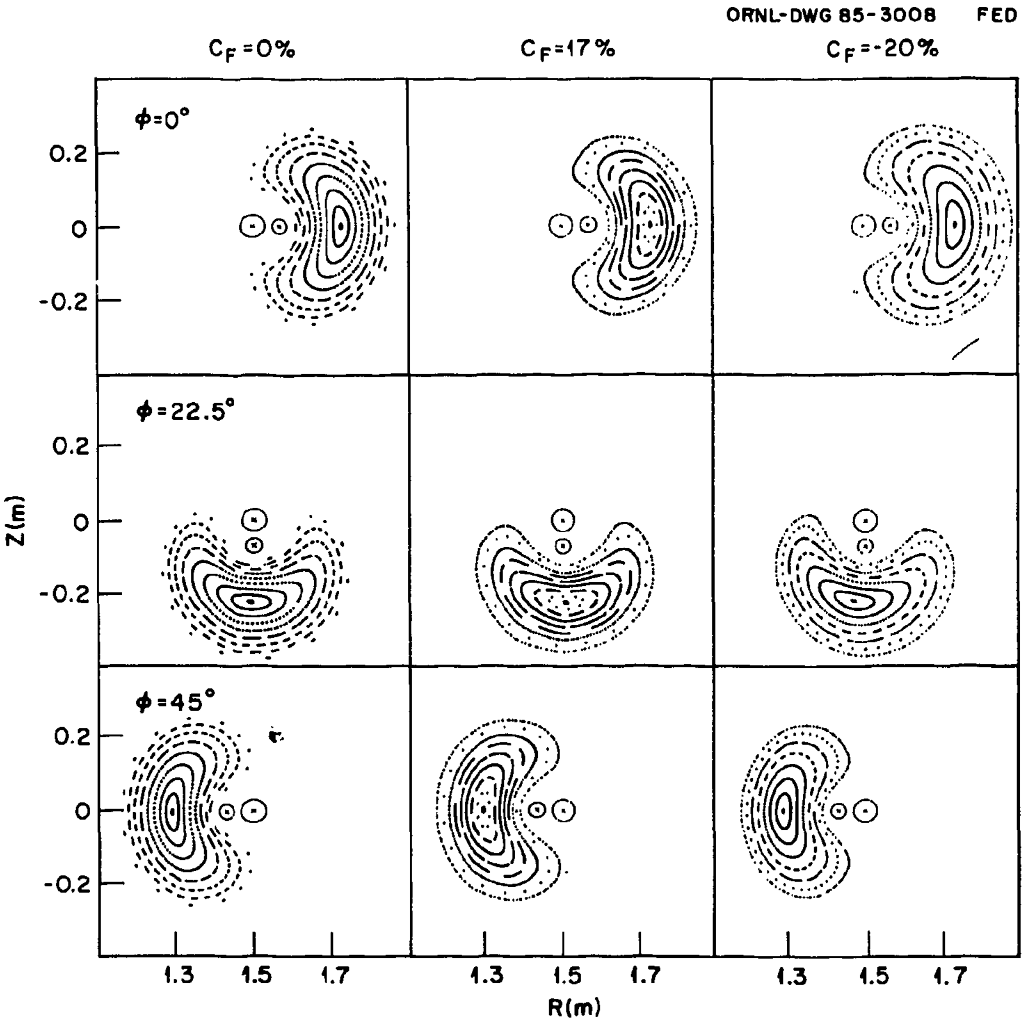

Fig. 15. Effect of TF coil current modulation on the flux surface shape.

where only the dominant helical terms are retained. The first term represents the uniform toroidal field, and the second term results from the average poloidal field generated by the hardcore windings. The Bessel function terms are related to the helical fields generated by the $\ell = 1$ hardcore winding (K_1 term) and the helical displacements of the TF coils (I_1 term). (This model has already been used in Ref. 1 to study some of the properties of the Flexible Heliac, and the formulas developed there are quoted and used without further proof.) The location of the magnetic axis $r = r_A$ is given by

$$\frac{r_A}{R_0} - \frac{\mu_0 I}{2\pi R_0 B_0}\frac{R_0}{r_A} = \frac{R_0}{r_A}\left(\frac{r_A^2}{R_0^2}+1\right)\left[\frac{a_1}{B_0}I_1\left(\frac{r_A}{R_0}\right) + \frac{b_1}{B_0}K_1\left(\frac{r_A}{R_0}\right)\right] \tag{3}$$

and the central transform by[11]

$$\frac{\iota_0}{M} = 1 - \frac{2e}{1+e^2}\frac{1}{(1+r_A^2/R_0^2)^{1/2}} , \tag{4}$$

where the ellipticity of surfaces is given by

$$e = \left\{\frac{\partial^2\psi}{\partial r^2}\Big/\left[\frac{1}{r_A^2}\frac{\partial^2\psi}{\partial\theta^2}\left(1+\frac{r_A^2}{R_0^2}\right)\right]\right\}^{1/2} . \tag{5}$$

Using these formulas, we can construct a contour plot equivalent to Fig. 6; Fig. 16 shows contours of constant ι_0/M as functions of b_1/B_0 and $\mu_0 I/(2\pi R_0 B_0)$ for $a_1/B_0 = 0.25$. Each constant ι_0/M contour is a parabola that turns over at increasingly high current (I) as ι_0/M is increased. In the 3-D analogue, the flux surfaces are broken at the extreme ends of the ι_0/M contours by physical interference with the coils. Thus the radiating contours in Fig. 6 are, in fact, short segments of a series of parabolas. The analytic model also reproduces the property that the magnetic axis shifts further out as the total central conductor current is raised at constant ι_0/M. Figure 17 demonstrates this for the case $\iota_0/M = 0.35$.

IV. ENGINEERING CONSIDERATIONS

In this section, aspects of the physics studies that are related to engineering considerations are briefly discussed. In particular, studies of error fields, finite cross-section conductors, and plasma-coil clearances are described.

The low shear inherent to the Heliac accentuates the effects of resonant or nearly resonant error fields. Even with no errors present, the regions near the major resonances ($\iota_0/M = 1/4$, $1/3$, $1/2$, ...) are inaccessible. Errors that break the four-fold symmetry are the most dangerous, since they introduce a whole new class of low-order resonances (Fig. 18). For the reference configuration, the most dangerous of these error-induced resonances are $\iota = 3/2$ and $5/2$. The even lower order resonances $\iota = 1/1$ and $2/1$ are already inaccessible resonances ($\iota = 4/4$ and $4/2$) in the error-free case, which has the four-fold symmetry.

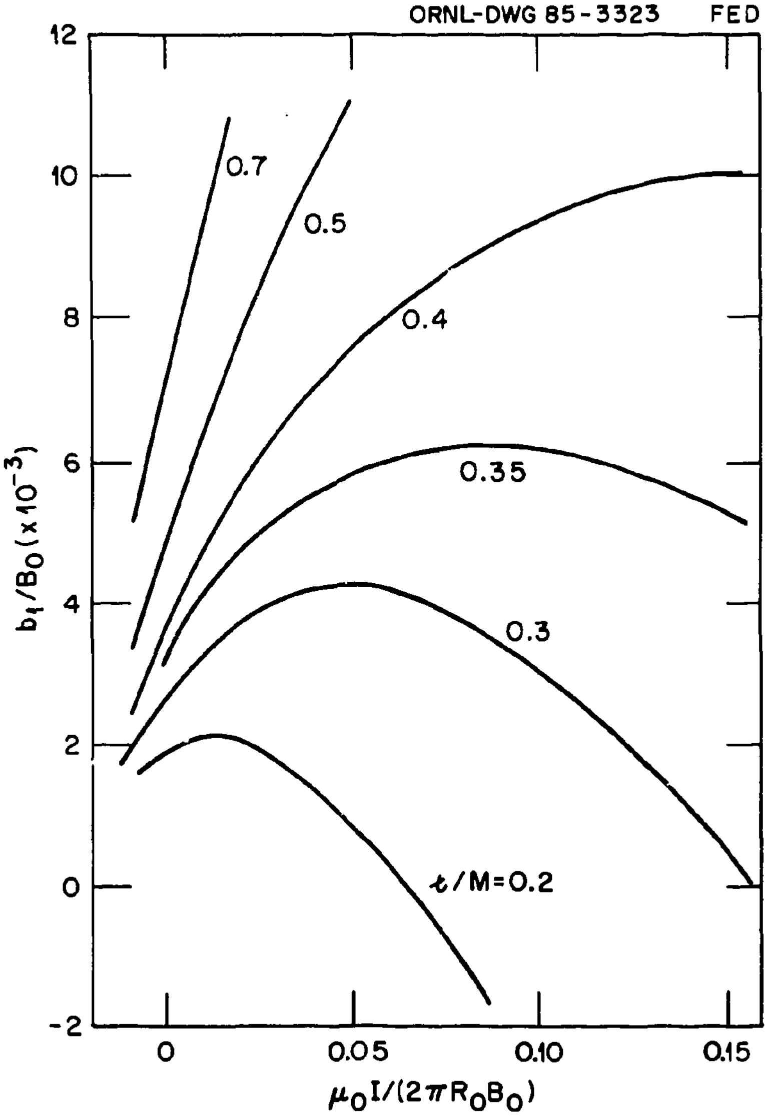

Fig. 16. Contours of ι_0/M from the analytical model.

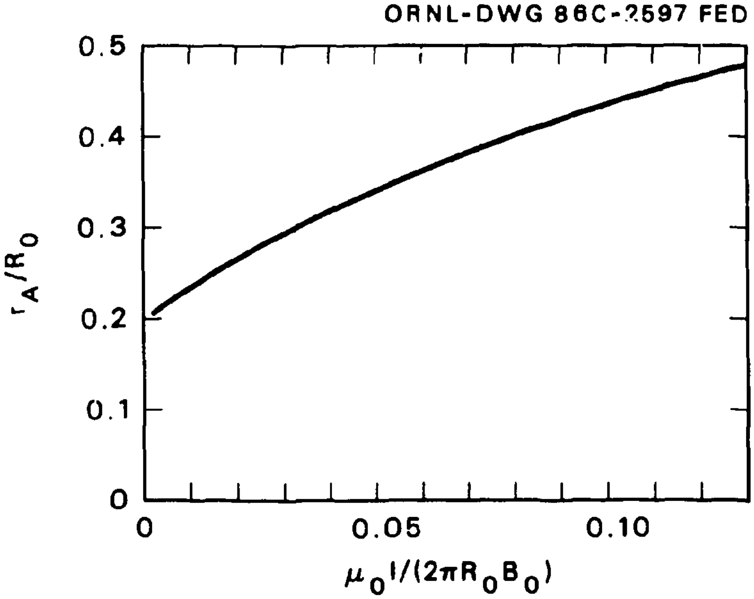

Fig. 17. Location of the magnetic axis (r_A) as the total current (I) is varied in the analytical model.

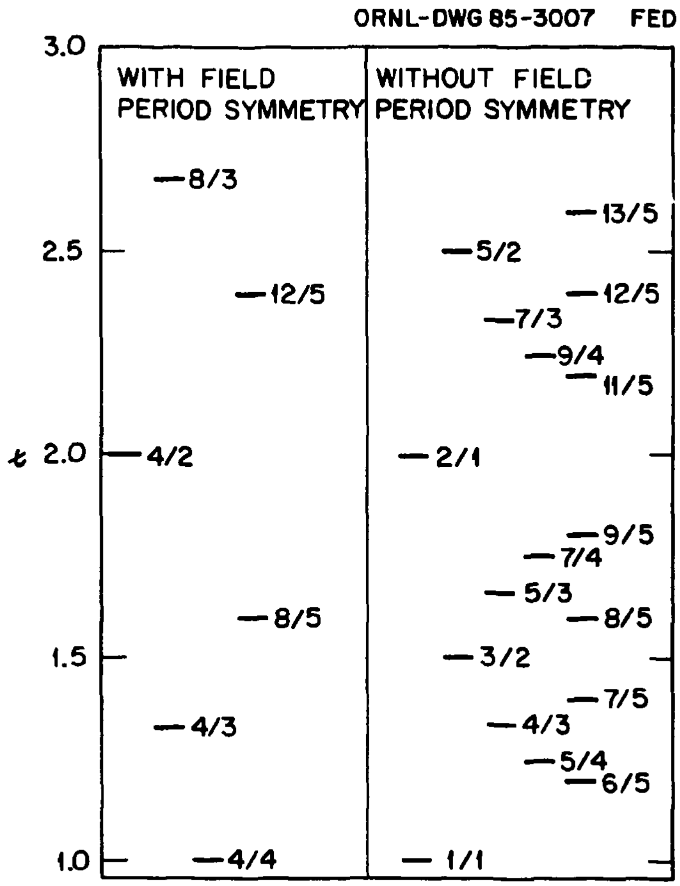

Fig. 18. Potential resonances with and without 4-field-period symmetry.

Figure 19 shows the effect of a horizontal offset of the central conductor structure relative to the TF coils; the unperturbed case has $\iota_0 = 1.46$, and the ι profile crosses the $\iota = 3/2$ resonance. For an offset of 2.5 mm, the $m = 2$ islands induced by the error fields are clearly visible. Other errors, such as gross tilts of the hardcore structure or distortions in the winding law of the $\ell = 1$ winding or TF coils, result in similar error tolerances.

The flexibility allows the resonance ($\iota = 3/2$) to be removed from the plasma by small changes in the hardcore currents. For a horizontal offset of 2.5 mm, changing the hardcore current by ~10% removes the $\iota = 3/2$ resonance and the associated error field problem (Fig. 20).

The effects of the error fields diminish rapidly for higher order resonances, because for higher poloidal mode numbers (m), the range of the error field (whose magnitude is $\propto x^{-m}$, where x is the distance from the source) decreases, and the island width associated with a given radial field perturbation ($\propto m^{-1/2}$) decreases.

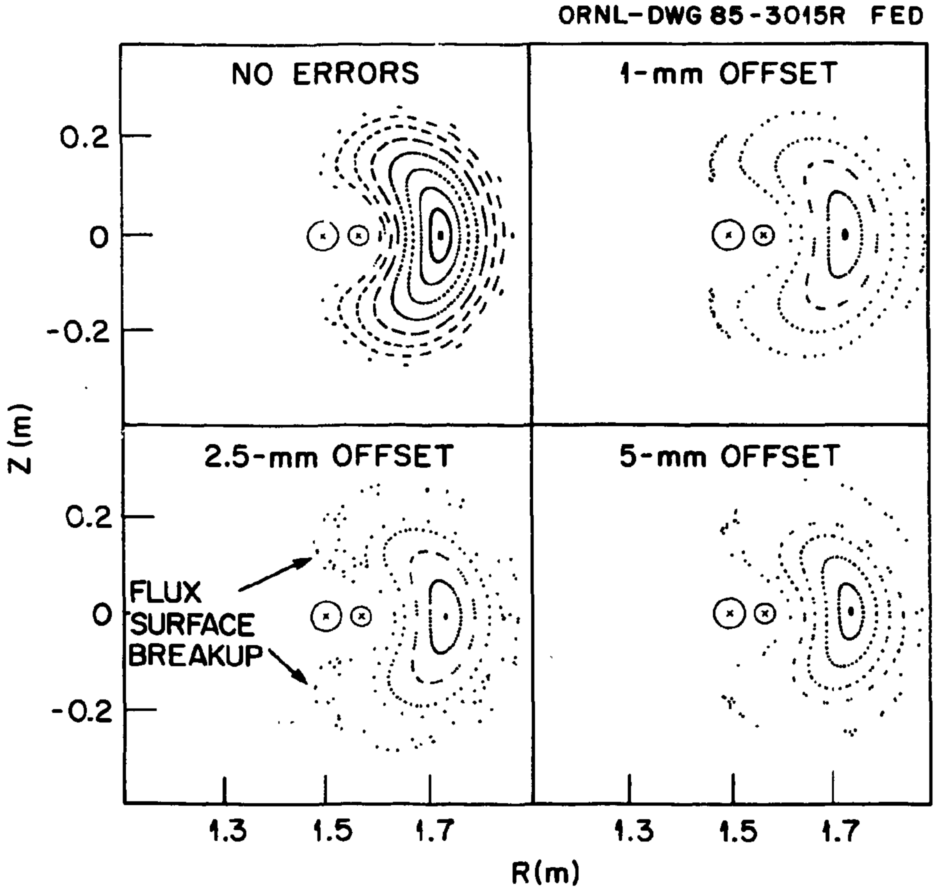

Fig. 19. Effect of various horizontal offsets of the central conductors relative to the TF coils ($\iota_0 = 1.46$).

ORNL-DWG 85-2929R FED

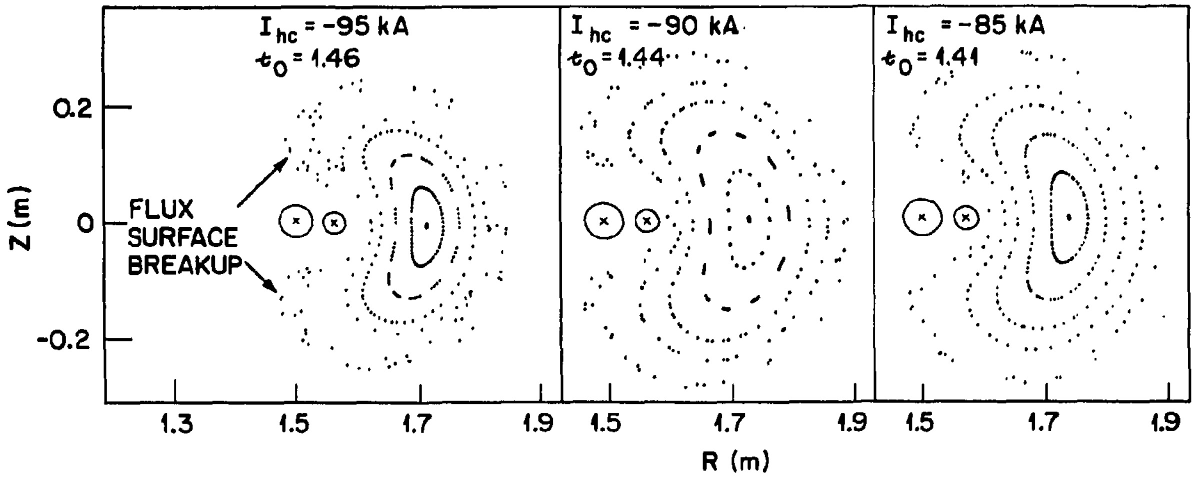

Fig. 20. Effect of lowering ι_0 to avoid having the $\iota = 3/2$ resonance in the plasma. The severe flux surface destruction caused by a 2.5-mm offset (Fig. 19 and left-hand flux surfaces in Fig. 20) can be avoided.

Figure 21 shows that, for a configuration containing the $\iota = 5/3$ resonance, a 2.5-mm offset of the hardcore has little effect on the flux surface quality; for the next order lower resonance, $\iota = 3/2$, this error is sufficient to destroy a large portion of the flux surfaces (Fig. 19). It should be noted, however, that the offset of the hardcore is more effective at generating $m = 2$ than $m = 3$ errors. There is a factor of ~2 reduction in island size in going from the $\iota = 3/2$ to the $\iota = 5/3$ resonance that can be directly attributed to the change in poloidal mode number. It becomes increasingly difficult to envisage physically feasible errors that would drive significant error fields of higher poloidal mode number.

The Flexible Heliac is remarkably robust with respect to errors that preserve the 4-field-period symmetry. For example, a possible support structure concept for the central conductor is a post three-fourths of the way through each field period (at this point the plasma is above the central conductor and access is possible). Even an average 3-cm "squaring" of the central conductor structure between these four 3/4-field-period fixed points leads only to a distortion of the plasma, with no significant loss of volume (Fig. 22). Such a squaring error is far beyond that likely to be caused by the magnetic forces.

The main conclusion of the error field studies is thus that errors that break the field period symmetry are the most troublesome. A tolerance of <1 mm is set by such errors, and even then, configurations with the $\iota = 5/2$ and $3/2$ resonances may be inaccessible. The configuration is very tolerant of errors that preserve the four-fold symmetry; this suggests that the support structures, etc., should all have this symmetry.

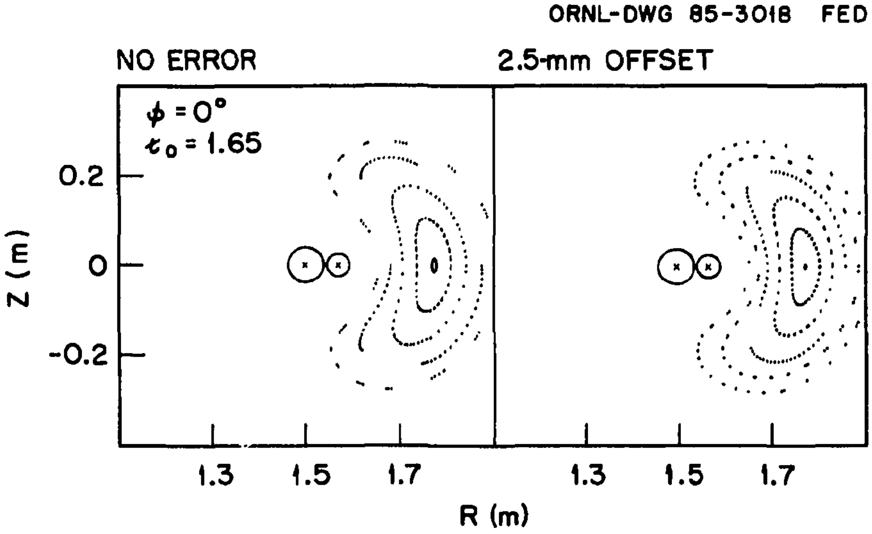

Fig. 21. For the $\iota = 5/3$ resonance, a 2.5-mm offset error causes no noticeable flux surface destruction.

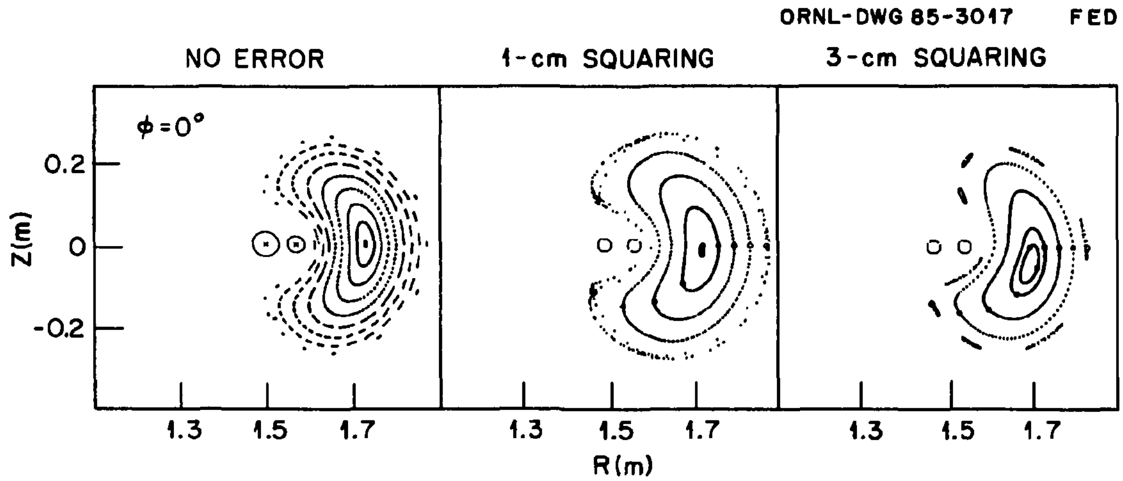

Fig. 22. Effect of squaring the central conductor structure about the fixed points $67.5° + M \times 90°$ ($M = 0, \ldots, 3$). The squaring is measured by the average deviation from circularity.

These results change very little when the effects of the finite cross section of the conductors are included. The finite-size coils are simulated by using increasingly large numbers of filaments uniformly distributed throughout the cross section of the coil. The effects of the finite cross-section central conductor (Fig. 23), $\ell = 1$ winding (Fig. 24), and TF coils (Fig. 25) have been checked for several cases. The impact of using finite coil sizes can be seen to be very small; comparison of sensitive quantities such as the magnetic well confirms this conclusion.

Finally, we consider the clearance between the plasma, the $\ell = 1$ winding, and the TF coils. Figure 26 shows the distance from each magnetic surface (labeled by its average radius) to the center of the $\ell = 1$ winding for several values of ι/M. The reference value for the cross-sectional radius of the $\ell = 1$ winding is 3.5 cm, so surfaces that are $\lesssim$3.5 cm from the helical winding center must be eliminated with a material limiter. It can be seen that each 1 cm of increased separation between the plasma and the $\ell = 1$ winding requires approximately a 2-cm reduction in average radius. Also, it can be seen that the high-ι/M (>0.5) configurations have considerably improved clearances.

There are several ways to improve the clearance between the plasma and the $\ell = 1$ winding. As discussed in Sec. III, if the hardcore current is increased at constant ι_0/M, the plasma shifts away from the central conductor structure, and there is an accompanying increase in plasma volume. This is illustrated in Fig. 27 for the $\iota_0/M = 0.36$ case. Another method of increasing the separation is to use a "poloidally spread" helical winding (Fig. 28). For the case illustrated, there is a 2.5-cm increase in clearance for flux surfaces having the same average radius. There is, however, a trade-off here, because poloidally spreading the $\ell = 1$ winding makes it less effective at generating the helical fields, and thus higher currents are required.

The other clearance of concern is that between the plasma and the TF coils. Figure 29 compares the plasma clearance to the TF coils and $\ell = 1$ winding for three values of ι_0. In this case the clearances are to the edges of the coils and not the centers. It can be seen that for the high-ι case ($\iota \gtrsim 2$), neither of the clearances is a particular problem, and for lower transform values the clearance to the edge of the $\ell = 1$ winding is always more restrictive. A potential method of increasing the TF coil clearance still further is to use square TF coils; this is illustrated in Fig. 30 for an $\iota_0/M = 0.3$ case.

V. SUMMARY

The Flexible Heliac reference configuration was determined by systematic parameter scans about a 4-field-period, $R = 1.5$ m case, the gross size of the device being set by considerations of economics and plasma minor radius.

The selected configuration allows the rotational transform to be varied by at least a factor of 5 ($0.15 \lesssim \iota_0/M \lesssim 0.8$). This flexibility, which greatly exceeds that of the standard Heliac, results from the addition of the $\ell = 1$ winding to the hardcore structure. At fixed ι_0/M, the magnetic well depth and plasma volume can be altered to a more limited extent by varying the mix of hardcore currents;

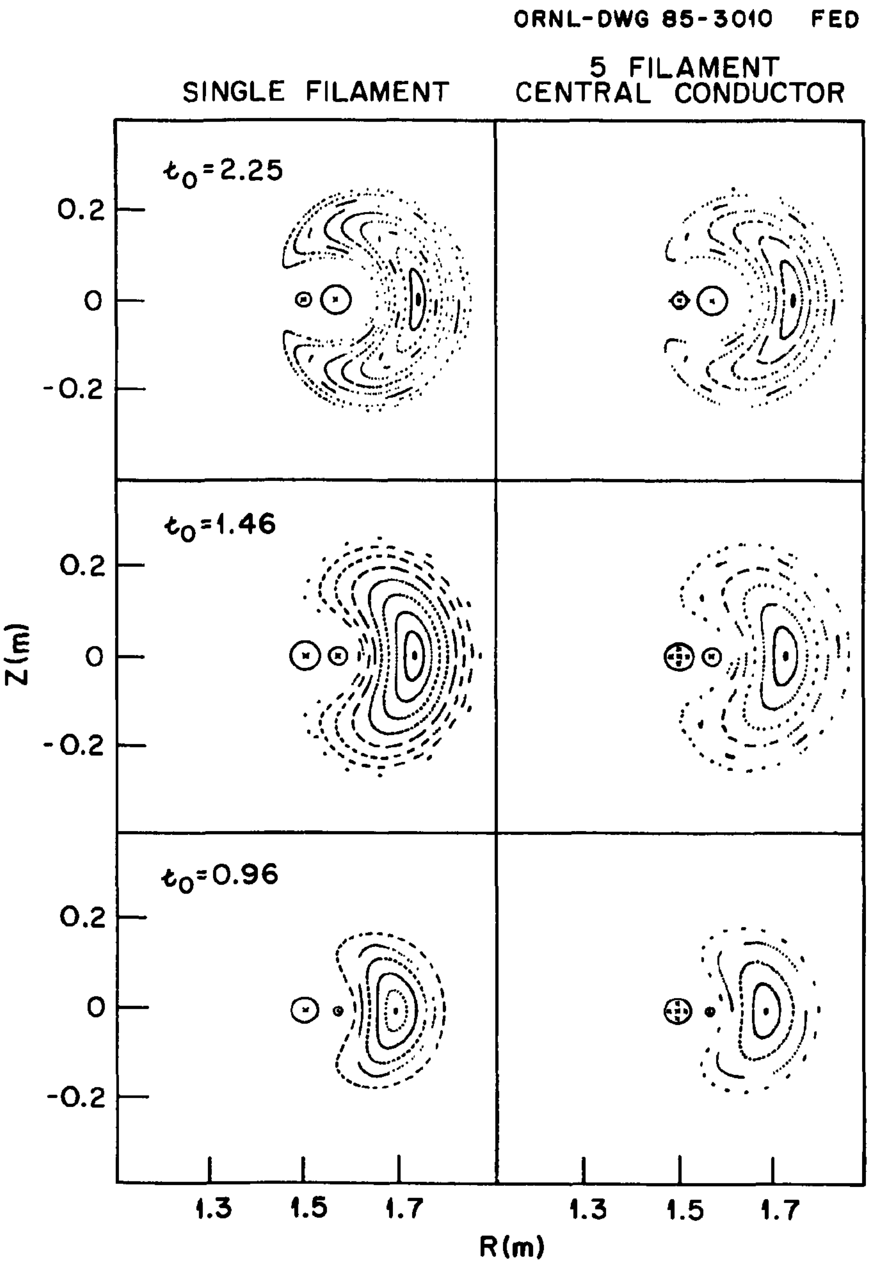

Fig. 23. Inclusion of a finite cross-section central conductor has no effect on the flux surfaces.

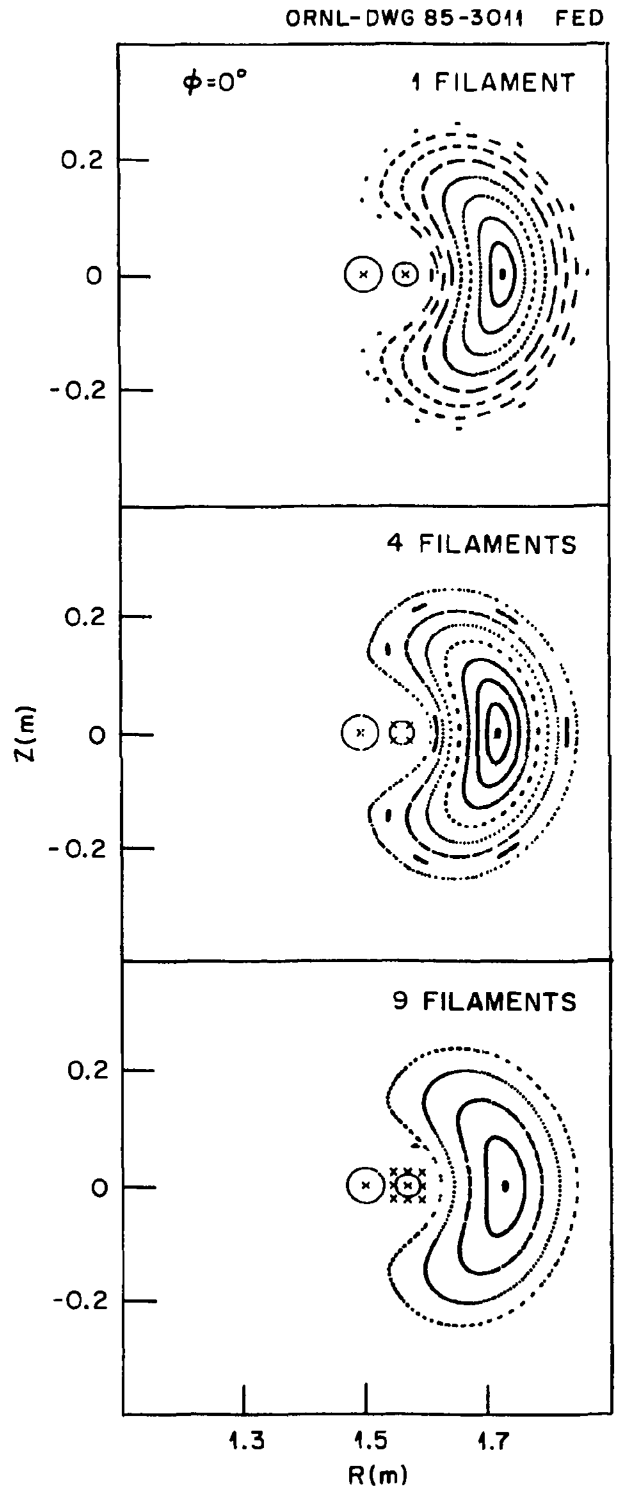

Fig. 24. A finite cross-section $\ell = 1$ winding produces no significant changes in the flux surface quality.

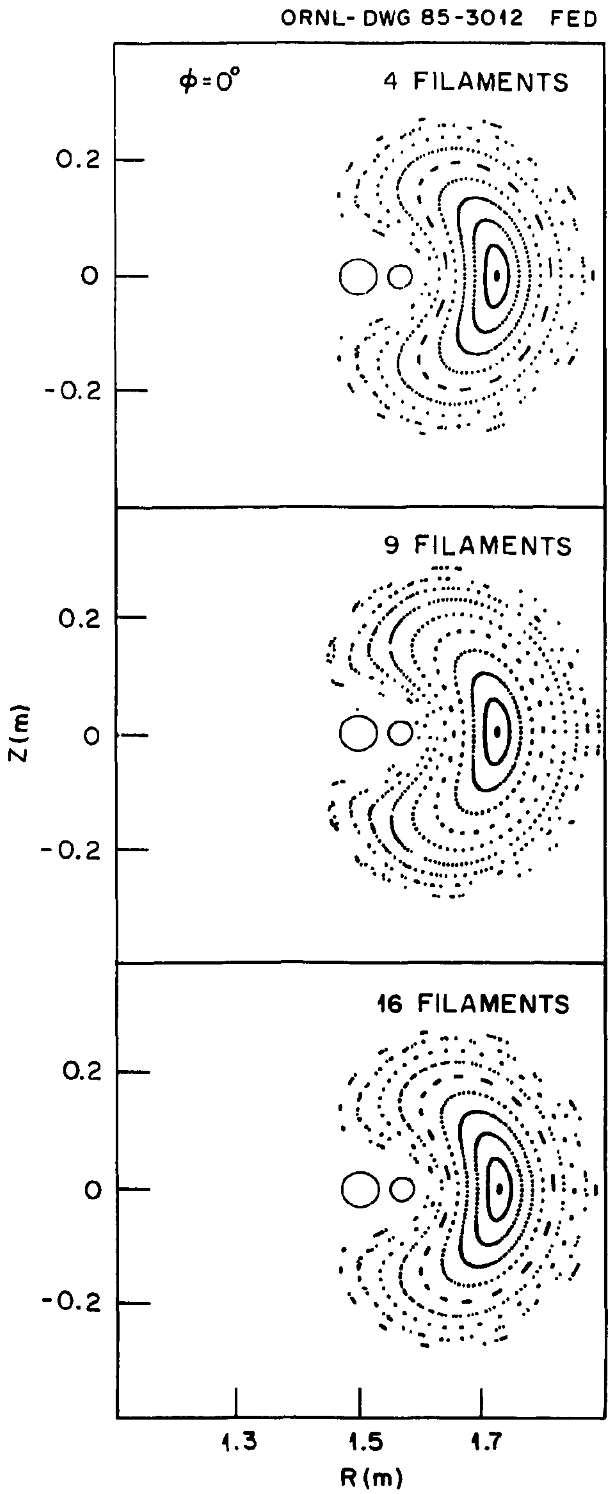

Fig. 25. Finite cross-section TF coils have very little effect on the flux surface quality.

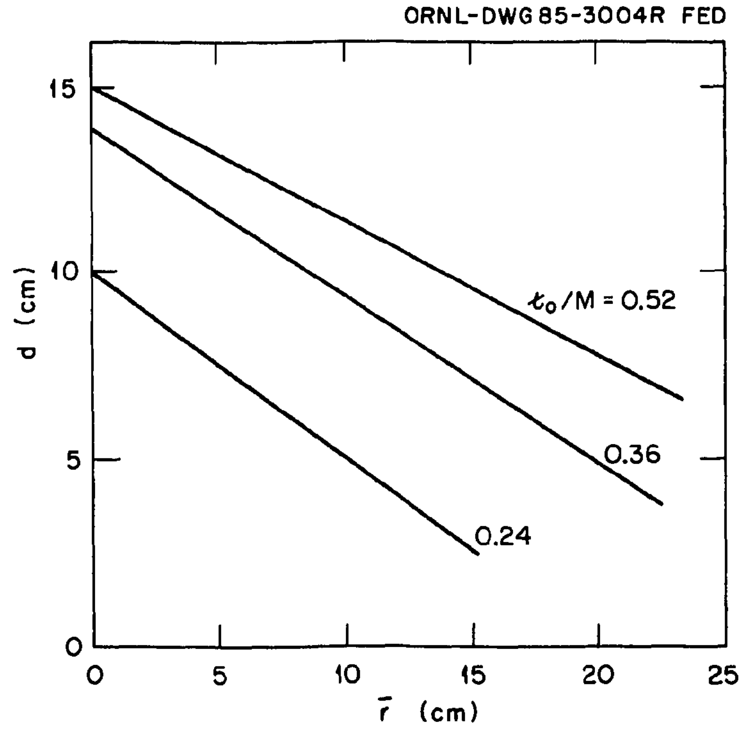

Fig. 26. Clearance to the center of the $\ell = 1$ winding as a function of average radius for various values of ι_0/M.

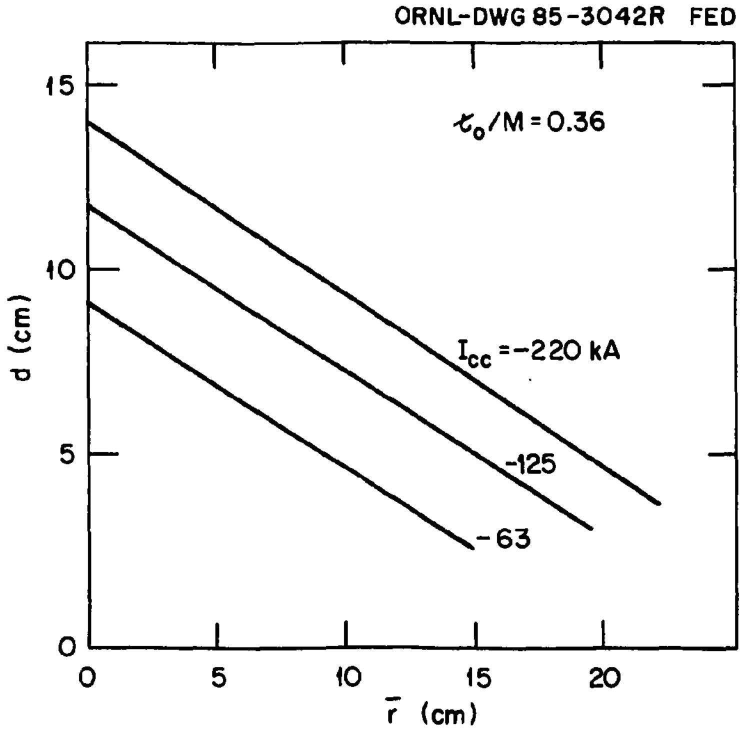

Fig. 27. Effect of increasing the central conductor currents at fixed ι_0/M. The clearance to the center of the $\ell = 1$ winding can be increased.

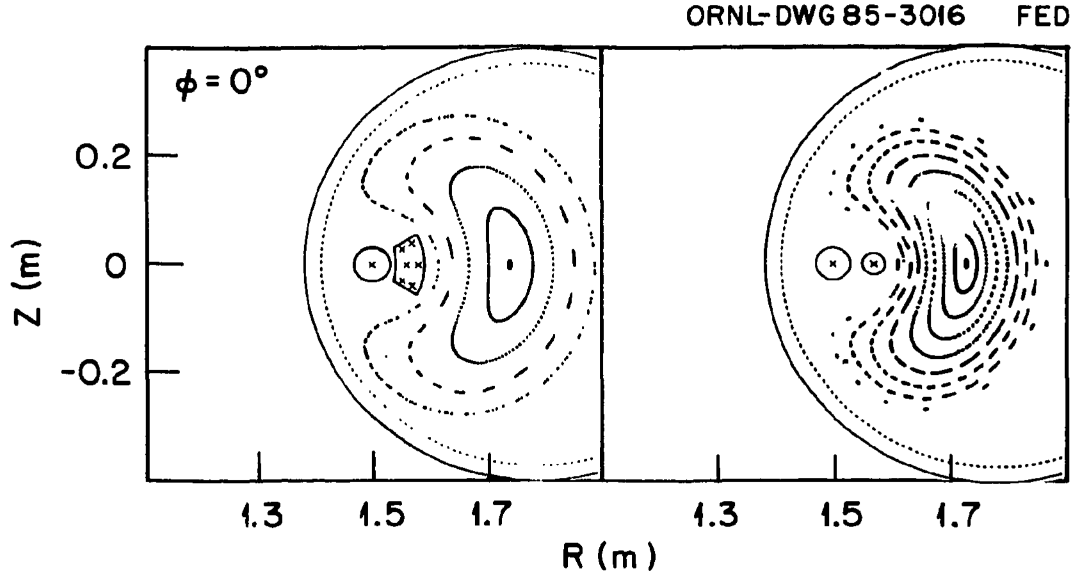

Fig. 28. Plasma clearance with a poloidally spread $\ell = 1$ winding (left) and with the circular cross-section $\ell = 1$ winding (right).

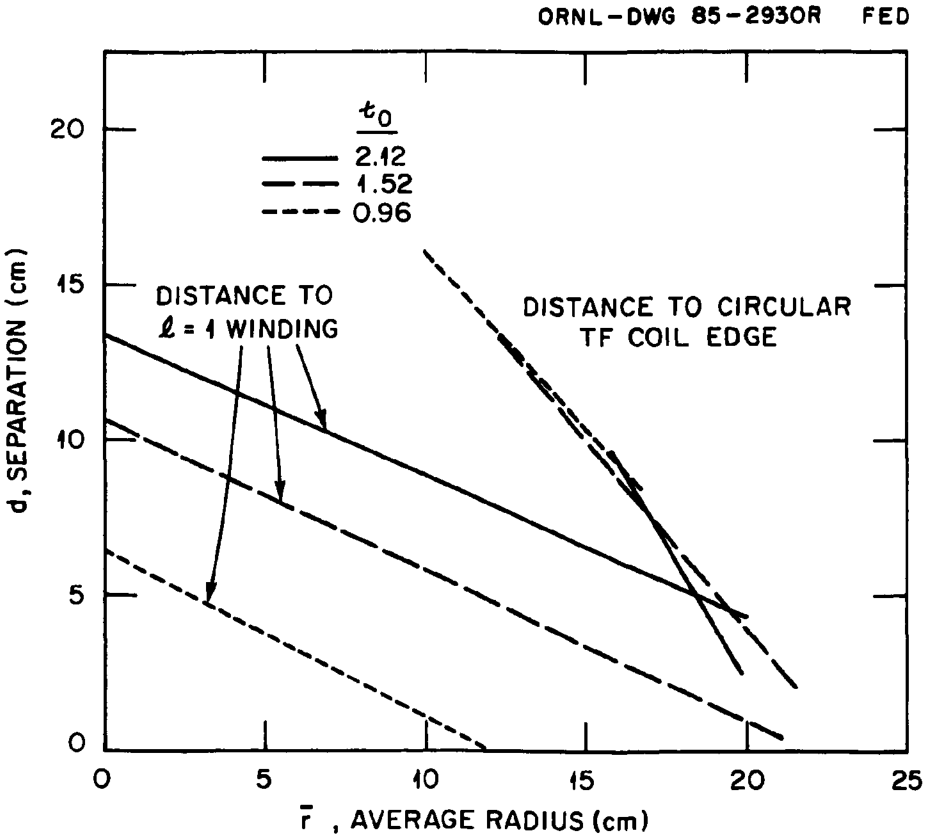

Fig. 29. Clearance between the edge of the $\ell = 1$ winding and the plasma and between the TF coils and the plasma.

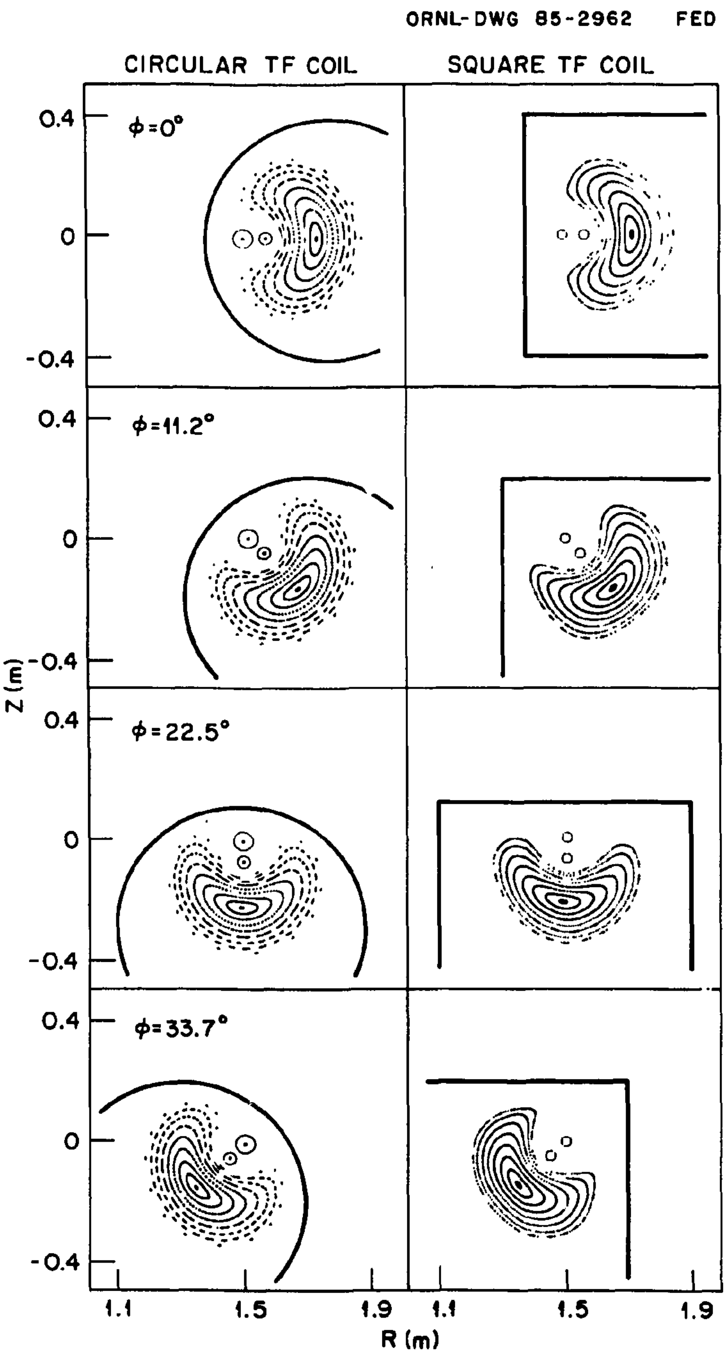

Fig. 30. Clearance between the plasma and the TF coils can be improved by using square TF coils.

plasmas with average minor radii up to 25 cm can be produced. A relatively large variation in the shear can be achieved by independently powering the inner and outer turns of the $\ell = 1$ winding, which permits the effective current center of the helical current to be shifted between 5.25 and 8.75 cm (for $I_{hc} \lesssim 150$ kA).

Error field studies have show that perturbations that break the four-fold symmetry are most serious since they excite low-order resonances. The effects of including the finite cross section of the conductors are small, even when sensitive quantities such as the magnetic well are compared.

The most important of the plasma coil clearances is that between the $\ell = 1$ winding and the plasma. This problem is particularly pronounced at low ι. It appears likely that some form of material limiter will be necessary to protect the $\ell = 1$ winding in these cases. The clearance to the $\ell = 1$ winding can be increased at a given ι by using higher hardcore currents. Poloidally spreading the $\ell = 1$ winding also improves this clearance.

In summary, the flexibility of the reference configuration allows the study of rotational transform values between those of conventional stellarators (~0.1/field period) and the very high values (~0.8/field period) that can only be achieved in helical-axis devices. The fine control over the transform, shear, and magnetic well afforded by this configuration should permit the study of the effects of resonances and improve theoretical understanding. By finely tuning the profiles to avoid equilibrium problems, it should be possible to gain access to high-beta stable regimes.

REFERENCES

1. J. H. HARRIS, J. L. CANTRELL, T. C. HENDER, B. A. CARRERAS, and R. N. MORRIS, "A Flexible Heliac Configuration," *Nucl. Fusion*, **25**, 623 (1985).

2. S. YOSHIKAWA, "Design of a Helical-Axis Stellarator," *Nucl. Fusion*, **23**, 667 (1983).

3. A. H. BOOZER, T. K. CHU, R. L. DEWAR, H. P. FURTH, J. A. GOREE, J. L. JOHNSON, R. M. KULSRUD, D. A. MONTICELLO, G. KUO-PETRAVIC, and S. YOSHIKAWA, "Two High-Beta Toroidal Configurations: A Stellarator and a Tokamak-Torsatron Hybrid," *Proc. 9th Int. Conf. Plasma Physics and Controlled Nuclear Fusion Research*, Baltimore, 1982, Vol. 3, p. 129, International Atomic Energy Agency, Vienna (1983).

4. D. A. MONTICELLO, R. L. DEWAR, H. P. FURTH, and A. REIMAN, "Heliac Parameter Study," *Phys. Fluids*, **27**, 1248 (1984).

5. A. REIMAN and A. H. BOOZER, "Island Formation and Destruction of Flux Surfaces in Three-Dimensional MHD Equilibria," *Phys. Fluids*, **27**, 2446 (1984).

6. B. A. CARRERAS, J. L. CANTRELL, L. A. CHARLTON, L. GARCIA, J. H. HARRIS, T. C. HENDER, H. R. HICKS, J. A. HOLMES, J. A. ROME, and V. E. LYNCH, "MHD Equilibrium and Stability for Stellarator/Torsatron," *Proc. 10th Int. Conf. Plasma Physics and Controlled Nuclear Fusion Research*, London, 1984, Vol. 2, p. 31, International Atomic Energy Agency, Vienna (1985).

7. J. R. CARY and M. KOTSCHENREUTHER, "Pressure Induced Islands in Three-Dimensional Toroidal Plasma," *Phys. Fluids*, **28**, 1392 (1985).

8. B. D. BLACKWELL, R. L. DEWAR, H. J. GARDNER, S. M. HAMBERGER, L. E. SHARP, X. H. SHI, C. F. VANCE, and D. F. ZHOU, "Experimental and Theoretical Studies of Toroidal Heliacs," paper DIII-6 presented at the 11th International Conference on Plasma Physics and Controlled Nuclear Fusion Research, Kyoto, November 1986 (proceedings to be published by the International Atomic Energy Agency, Vienna, 1987).

9. A. PEREA, J. L. ALVAREZ-RIVAS, J. BOTIJA, J. R. CEPERO, et al., "Physics Issues in the Design of TJ-II," *Proc. 12th European Conf. Controlled Fusion and Plasma Physics*, Budapest, Hungary, 1985, *Europhysics Conf. Abstr. Ser.* **9F**, Part I, p. 433, European Physical Society (1985).

10. T. C. HENDER, B. A. CARRERAS, and V. E. LYNCH, "Heliac Equilibria," Oak Ridge National Laboratory Report ORNL/TM-10171, 1986.

11. B. McNAMARA, K. J. WHITEMAN, and J. B. TAYLOR, "Helical Fields Possessing Mean Magnetic Wells," *Proc. Conf. Plasma Physics and Controlled Nuclear Fusion Research*, Culham, 1965, Vol. 1, p. 145, International Atomic Energy Agency, Vienna (1966).

12. N. M. ZUEVA and L. S. SOLOV'EV, "Spiral Magnetic Configurations with Minimum $\bar{B}^*$," *Plasma Phys.*, **8**, 765 (1966).

13. H. P. FURTH, J. KILLEEN, M. N. ROSENBLUTH, and B. COPPI, "Stabilization by Shear and Negative V''," *Proc. Conf. Plasma Physics and Controlled Nuclear Fusion Research*, Culham, 1965, Vol. 1, p. 103, International Atomic Energy Agency, Vienna (1966).

ORNL/TM-10374
Dist. Category UC-20

INTERNAL DISTRIBUTION

1.	L. A. Berry	33.	G. H. Neilson
2–5.	J. L. Cantrell	34.	D. A. Rasmussen
6–10.	B. A. Carreras	35.	J. A. Rome
11.	R. J. Colchin	36.	M. J. Saltmarsh
12.	R. A. Dory	37.	J. Sheffield
13.	J. L. Dunlap	38–39.	Laboratory Records Department
14.	A. C. England	40.	Laboratory Records, ORNL-RC
15.	R. H. Fowler	41.	Document Reference Section
16–20.	J. H. Harris	42.	Central Research Library
21.	T. C. Jernigan	43.	Fusion Energy Division Library
22–26.	V. E. Lynch	44–45.	Fusion Energy Division Publications Office
27–31.	J. F. Lyon	46.	ORNL Patent Office
32.	M. Murakami		

EXTERNAL DISTRIBUTION

47–51. T. C. Hender, Culham Laboratory, Abingdon, Oxon OX14 3DB, England

52. J. A. Fabregas, Division de Fusion, Asociacion EURATOM/CIEMAT, Junta de Energia Nuclear, 28040 Madrid, Spain

53. J. Guasp, Division de Fusion, Asociacion EURATOM/CIEMAT, Junta de Energia Nuclear, 28040 Madrid, Spain

54. A. Lopez-Fraguas, Division de Fusion, Asociacion EURATOM/CIEMAT, Junta de Energia Nuclear, 28040 Madrid, Spain

55. A. P. Navarro, Division de Fusion, Asociacion EURATOM/CIEMAT, Junta de Energia Nuclear, 28040 Madrid, Spain

56. Office of the Assistant Manager for Energy Research and Development, U.S. Department of Energy, Oak Ridge Operations Office, P. O. Box E, Oak Ridge, TN 37831

57. J. D. Callen, Department of Nuclear Engineering, University of Wisconsin, Madison, WI 53706-1687

58. J. F. Clarke, Director, Office of Fusion Energy, Office of Energy Research, ER-50 Germantown, U.S. Department of Energy, Washington, DC 20545

59. R. W. Conn, Department of Chemical, Nuclear, and Thermal Engineering, University of California, Los Angeles, CA 90024

60. S. O. Dean, Fusion Power Associates, Inc., 2 Professional Drive, Suite 249, Gaithersburg, MD 20760

61. H. K. Forsen, Bechtel Group, Inc., Research Engineering, P. O. Box 3965, San Francisco, CA 94105
62. J. R. Gilleland, GA Technologies, Inc., Fusion and Advanced Technology, P.O. Box 81608, San Diego, CA 92138
63. R. W. Gould, Department of Applied Physics, California Institute of Technology, Pasadena, CA 91125
64. R. A. Gross, Plasma Research Laboratory, Columbia University, New York, NY 10027
65. D. M. Meade, Princeton Plasma Physics Laboratory, P.O. Box 451, Princeton, NJ 08544
66. M. Roberts, International Programs, Office of Fusion Energy, Office of Energy Research, ER-52 Germantown, U.S. Department of Energy, Washington, DC 20545
67. W. M. Stacey, School of Nuclear Engineering and Health Physics, Georgia Institute of Technology, Atlanta, GA 30332
68. D. Steiner, Nuclear Engineering Department, NES Building, Tibbetts Avenue, Rensselaer Polytechnic Institute, Troy, NY 12181
69. R. Varma, Physical Research Laboratory, Navrangpura, Ahmedabad 380009, India
70. Bibliothek, Max-Planck Institut fur Plasmaphysik, D-8046 Garching, Federal Republic of Germany
71. Bibliothek, Institut fur Plasmaphysik, KFA, Postfach 1913, D-5170 Julich, Federal Republic of Germany
72. Bibliotheque, Centre de Recherches en Physique des Plasmas, 21 Avenue des Bains, 1007 Lausanne, Switzerland
73. F. Prevot, CEN/Cadarache, Departement de Recherches sur la Fusion Controlee, F-13108 Saint-Paul-lez-Durance Cedex, France
74. Documentation S.I.G.N., Departement de la Physique du Plasma et de la Fusion Controlee, Centre d'Etudes Nucleaires, B.P. 85, Centre du Tri, F-38041 Grenoble, France
75. Library, Culham Laboratory, UKAEA, Abingdon, Oxfordshire, OX14 3DB, England
76. Library, FOM-Instituut voor Plasma-Fysica, Rijnhuizen, Edisonbaan 14, 3439 MN Nieuwegein, The Netherlands
77. Library, Institute of Plasma Physics, Nagoya University, Nagoya 464, Japan
78. Library, International Centre for Theoretical Physics, P.O. Box 586, I-34100 Trieste, Italy
79. Library, Laboratorio Gas Ionizatti, CP 56, I-00044 Frascati, Rome, Italy
80. Library, Plasma Physics Laboratory, Kyoto University, Gokasho, Uji, Kyoto, Japan
81. Plasma Research Laboratory, Australian National University, P.O. Box 4, Canberra, A.C.T. 2000, Australia

82. Thermonuclear Library, Japan Atomic Energy Research Institute, Tokai Establishment, Tokai-mura, Naka-gun, Ibaraki-ken, Japan
83. G. A. Eliseev, I. V. Kurchatov Institute of Atomic Energy, P. O. Box 3402, 123182 Moscow, U.S.S.R.
84. V. A. Glukhikh, Scientific-Research Institute of Electro-Physical Apparatus, 188631 Leningrad, U.S.S.R.
85. I. Shpigel, Institute of General Physics, U.S.S.R. Academy of Sciences, Ulitsa Vavilova 38, Moscow, U.S.S.R.
86. D. D. Ryutov, Institute of Nuclear Physics, Siberian Branch of the Academy of Sciences of the U.S.S.R., Sovetskaya St. 5, 630090 Novosibirsk, U.S.S.R.
87. V. T. Tolok, Kharkov Physical-Technical Institute, Academical St. 1, 310108 Kharkov, U.S.S.R.
88. Library, Academia Sinica, P.O. Box 3908, Beijing, China (PRC)
89. R. A. Blanken, Experimental Plasma Research Branch, Division of Applied Plasma Physics, Office of Fusion Energy, Office of Energy Research, ER-542, Germantown, U.S. Department of Energy, Washington, DC 20545
90. K. Bol, Princeton Plasma Physics Laboratory, P.O. Box 451, Princeton, NJ 08544
91. R. A. E. Bolton, IREQ Hydro-Quebec Research Institute, 1800 Montee Ste.-Julie, Varennes, P.Q. JOL 2P0, Canada
92. D. H. Crandall, Experimental Plasma Research Branch, Division of Applied Plasma Physics, Office of Fusion Energy, Office of Energy Research, ER-542, Germantown, U.S. Department of Energy, Washington, DC 20545
93. R. L. Freeman, GA Technologies, Inc., P.O. Box 81608, San Diego, CA 92138
94. K. W. Gentle, RLM 11.222, Institute for Fusion Studies, University of Texas, Austin, TX 78712
95. R. J. Goldston, Princeton Plasma Physics Laboratory, P.O. Box 451, Princeton, NJ 08544
96. J. C. Hosea, Princeton Plasma Physics Laboratory, P.O. Box 451, Princeton, NJ 08544
97. S. W. Luke, Division of Confinement Systems, Office of Fusion Energy, Office of Energy Research, ER-55, Germantown, U.S. Department of Energy, Washington, DC 20545
98. E. Oktay, Division of Confinement Systems, Office of Fusion Energy, Office of Energy Research, ER-55, Germantown, U.S. Department of Energy, Washington, DC 20545
99. D. Overskei, GA Technologies, Inc., P.O. Box 81608, San Diego, CA 92138
100. R. R. Parker, Plasma Fusion Center, NW 16-288, Massachusetts Institute of Technology, Cambridge, MA 02139
102. W. L. Sadowski, Fusion Theory and Computer Services Branch, Division of Applied Plasma Physics, Office of Fusion Energy, Office of Energy Research, ER-541, Germantown, U.S. Department of Energy, Washington, DC 20545

103. J. W. Willis, Division of Confinement Systems, Office of Fusion Energy, Office of Energy Research, ER-55, Germantown, U.S. Department of Energy, Washington, DC 20545
104. Laboratory for Plasma and Fusion Studies, Department of Nuclear Engineering, Seoul National University, Shinrim-dong, Gwanak-ku, Seoul 151, Korea
105. J. L. Johnson, Plasma Physics Laboratory, Princeton University, P.O. Box 451, Princeton, NJ 08544
106. L. M. Kovrizhnykh, Institute of General Physics, U.S.S.R. Academy of Sciences, Ulitsa Vavilova 38, 117924 Moscow, U.S.S.R.
107. O. Motojima, Plasma Physics Laboratory, Kyoto University, Gokasho, Uji, Kyoto, Japan
108. V. D. Shafranov, I. V. Kurchatov Institute of Atomic Energy, P.O. Box 3402, 123182 Moscow, U.S.S.R.
109. J. L. Shohet, Torsatron/Stellarator Laboratory, University of Wisconsin, Madison, WI 53706
110. H. Wobig, Max-Planck Institut fur Plasmaphysik, D-8046 Garching, Federal Republic of Germany

111–188. Given distribution as shown in TIC-4500, Magnetic Fusion Energy (Distribution Category UC-20)